https://doi.org/10.5194/egusphere-2026-343
Preprint. Discussion started: 3 March 2026

Random forest parameterization of Antarctic subglacial hydrology for coupled ice-flow modelling

Tim Hill[1], Matthew J. Hoffman[2], Gwenn E. Flowers[1], and Derek Bingham[3]

[1]Department of Earth Sciences, Simon Fraser University, Burnaby, BC, Canada
[2]Fluid Dynamics and Solid Mechanics Group, Los Alamos National Laboratory, Los Alamos, NM, USA
[3]Department of Statistics and Actuarial Science, Simon Fraser University, Burnaby, BC, Canada

Correspondence: Tim Hill (tim_hill_2@sfu.ca)

Abstract. Antarctic ice-sheet flow is sensitive to changes in basal friction. These frictional changes are modulated by the effective pressure in the subglacial drainage system in response to changes in ice thickness, basal melt, and slip rates. To overcome the computational burden of coupled modelling of the ice sheet and the subglacial drainage system, we develop and evaluate a machine-learning parameterization of basal effective pressure. The parameterization, consisting of a random forest regression model, is trained to predict continent-wide effective pressure based on ensembles of simulations with the physics-based Glacier Drainage System (GlaDS) model in seven major ice-flow basins. The ensembles vary the values of five subglacial drainage model parameters, allowing the parameterization to predict how effective pressure varies across parameter space. The random forest parameterization explains 65% of the variance of the effective pressure predicted by the numerical model, but 99% of the variance in ice speed when coupled to the ice-flow solver in the Ice-Sheet and Sea-level System (ISSM) model. We assess the influence of effective pressure on future flow speeds by imposing plausible ice-sheet thickness changes drawn from ice-sheet model projections. Using the random forest parameterization instead of the numerical subglacial drainage model results in differences in grounding line speed of 127–311 m a^{-1} (2.1–10%). Other approaches, such as holding effective pressure constant in time or assuming ocean connectivity, result in larger grounding-line speed differences of 441–2199 m a^{-1} (8.5–74%). These results suggest that the random forest parameterization for effective pressure can be used to add active subglacial hydrology to ice-sheet modelling with higher fidelity than other effective-pressure parameterizations while reducing computation time from as long as 16 days to 0.5 seconds.

1 Introduction

Basal drag is a key component of ice-sheet force balance. Crucially, basal drag depends on effective pressure, which is modulated by subglacial drainage. Sensitivity studies show that the rate and magnitude of future mass loss from the Antarctic Ice Sheet depends on effective pressure and the basal friction parameterization near retreating grounding lines (e.g., Joughin et al., 2010; Pelle et al., 2024), with widely varying and basin-specific sensitivity (e.g., Zhao et al., 2025).

Predicting co-evolving effective pressure and ice-sheet geometry necessitates coupling hydrology and dynamics models. A variety of hydrology models are available, from fast, simplified models (e.g., Lu and Kingslake, 2024; Kazmierczak et al., 2024; de Fleurian et al., 2014; Fischler et al., 2023) to more complex models that aim to represent the physics of efficient flow

https://doi.org/10.5194/egusphere-2026-343
Preprint. Discussion started: 3 March 2026

through subglacial channels (e.g., Werder et al., 2013; Sommers et al., 2018; Hoffman et al., 2018). While basin-scale models accounting for certain hydrology–ice-flow feedbacks are becoming feasible (e.g., Pelle et al., 2023), fully coupled models appropriate for long-term continental-scale simulations remain computationally out of reach with all but the simplest hydrology models. Instead of including active subglacial drainage, ice-sheet models resort to simple parameterization of effective pressure, such as assuming hydraulic connection to the ocean (e.g., Asay-Davis et al., 2016; Brondex et al., 2019). Other models subsume effective pressure into the basal friction coefficient, with or without parameterized reductions in friction near the grounding line based on the height of ice above flotation (e.g., Joughin et al., 2010, 2019). Alternative approaches have included site-specific algebraic parametrizations (McArthur et al., 2023), combining height-above-flotation scaling with simulated effective pressure fields (Zhao et al., 2025), assuming effective pressure is uniformly 5% of ice overburden (Ma et al., 2025), and parameterizing a smooth transition between perfect-ocean-connection and fraction-of-overburden assumptions (Downs and Johnson, 2022). While these fast but simplified models present yet another path forward, they miss potentially important details of realistic effective pressure fields compared to the class of multi-component physics-based models (e.g., Werder et al., 2013; Sommers et al., 2018; Hoffman et al., 2018).

To address the limitations of effective-pressure parameterizations while avoiding the computational burden associated with coupling physics-based drainage models with ice flow, we present a statistical parameterization of Antarctic subglacial effective pressure. The parameterization is trained on a large ensemble of basin-scale simulations with a numerical subglacial drainage model. We combine the statistical parameterization with diagnostic solutions of ice velocity to investigate how the acceleration of grounded ice from the present-day to 2300 depends on the parameterization of effective pressure.

2 Methods

Our approach to parameterizing Antarctic subglacial effective pressure is to train a machine-learning model to approximate the Glacier Drainage System (GlaDS) (Werder et al., 2013) physics-based subglacial drainage model. The parameterization predicts effective pressure as a function of GlaDS model parameter values, local characteristics describing ice-sheet geometry, and forcing fields of the drainage model. Being based on local characteristics, the parameterization is not specific to a single region. We start by running an ensemble of GlaDS simulations for seven key Antarctic ice-flow basins and for a range of parameter values. This ensemble is used to train a random forest regression model (Breiman, 2001), which is used to make continent-wide predictions. We evaluate the effective pressures predicted by the random forest parameterization for present-day and representative future ice-sheet geometries against those predicted by the GlaDS model. Finally, by solving the stress balance using the Ice-sheet and Sea-level System Model (ISSM) (Larour et al., 2012) forced with our effective pressure fields, we evaluate the fidelity of the modelled ice-sheet velocity using the effective pressure parameterization relative to using effective pressure from the GlaDS model for plausible future ice-sheet states.

https://doi.org/10.5194/egusphere-2026-343
Preprint. Discussion started: 3 March 2026

Table 1. Model parameters and their ranges for the ensembles of GlaDS simulations

	Parameter	Value	Units
k_s	Sheet conductivity	[0.01, 1.0]	$\mathrm{Pa\,s^{-1}}$
k_c	Channel conductivity	[0.005, 0.5]	$\mathrm{m^{\frac{3}{2}}\,s^{-1}}$
r_b	Bed bump aspect ratio	[10, 100]	–
E_{creep}	Enhancement factor for creep closure	[0.1, 10]	–
l_c	Width of sheet beneath channels	[1, 100]	m

2.1 Physics-based subglacial drainage model

The GlaDS model (Werder et al., 2013) represents subglacial water flow through coupled linked cavity (Kamb, 1987) and channelized (Röthlisberger, 1972) drainage systems. Linked cavity drainage is parameterized as an area-averaged continuous water sheet that opens by sliding over bed bumps and closes by ice creep of the cavity roof (Schoof et al., 2012). Channelized drainage is modelled as one-dimensional channels that open by melt of the ice walls and close by creep (Hewitt et al., 2012). These systems are coupled by assuming a continuous hydraulic potential, and closure of the equations is obtained by including parameterizations for the discharge in each system. We use a parameterization for sheet flow that includes both laminar and turbulent flow (Hill et al., 2024), while retaining the standard turbulent flow parameterization for channels. By solving the coupled systems of equations, GlaDS calculates the hydraulic potential, area-averaged cavity height, and the cross-sectional area of subglacial channels. Secondary quantities, such as the effective pressure to be used in basal friction parameterizations, water pressure, or the flotation fraction, are computed from the hydraulic potential solution and ice-sheet geometry. We focus on the effective pressure N as the relevant variable for ice-sheet modelling. GlaDS parameters we hold fixed are listed in Table A2 and the ensemble design is discussed in Section 2.2.1 and summarized in Table 1. Based on the sensitivity of subglacial drainage to the ice-flow coefficient in the flow law (Hill et al., 2025b), we use separate coefficients controlling the rate of shear deformation used in the ice-sheet model (Section 2.4) and creep closure used in the hydrology model, with the creep-closure coefficient multiplied by an enhancement factor E_{creep}. We prohibit cavities from opening by creep when water pressures exceeds ice overburden pressure, which acts to cap cavity size at a value near the bed bump height. This choice disables active lake filling and draining, a major characteristic of Antarctic subglacial hydrology (e.g., Livingstone et al., 2022), to avoid training the statistical parameterization on transient behaviour. We use the version of GlaDS implemented within ISSM v4.24 (Section 2.4).

2.1.1 Ice-sheet geometry

As input for the subglacial drainage model, we take the ice-sheet bed elevation and ice thickness from BedMachine Antarctica v3 (Morlighem et al., 2020), which nominally represents conditions in 2015. We partition the ice sheet according to major ice-flow basins (Rignot et al., 2011b, a) (Fig. 1). The numerical domain for each basin consists of both grounded ice and ice

https://doi.org/10.5194/egusphere-2026-343
Preprint. Discussion started: 3 March 2026

shelves, with the ice front determined by the BedMachine Antarctica v3 ice–ocean mask (Morlighem et al., 2020). For the Filchner-Ronne ice-flow basins (Ellsworth Land, J-Jpp; Recovery ice-stream basin, Jpp-K) and the Siple coast (Ep-F), the hydrology model is solved on meshes containing grounded ice only.

For each basin, we construct a triangular numerical mesh with a nominal edge length of 2.5 km where surface speed is at least $50\,\mathrm{m\,a^{-1}}$ that transitions to 25 km in slower interior regions. This resolution is comparable to the 1.5–50 km resolution used by Ehrenfeucht et al. (2025) for Antarctic-wide hydrology modelling and 4–14 km used by Hager et al. (2022) for the Amundsen sea region, and somewhat coarser than 0.8–20 km used by Pelle et al. (2024) for regional coupled hydrology–dynamics simulations. The meshes in this study range in size from 23,375 nodes (basin J-Jpp) to 37,016 nodes (basin Jpp-K; see labels in Fig. 1(a)). Boundary conditions for the subglacial drainage model consist of a no-flux Neumann condition along interior boundaries and a flotation condition at the grounding line.

2.1.2 Forcing

GlaDS is forced with the spatially varying basal melt rates and basal slip speeds used by the subglacial drainage simulations of Vaňková et al. (2025), which are derived from the ice-sheet model initialization of Hillebrand et al. (2025b). In that initialization, ice-sheet basal friction and ice stiffness were calibrated through a PDE-constrained optimization to yield an ice velocity field, and consistent steady-state temperature field, that matches observed surface velocity. Following Vaňková et al. (2025), we use the basal slip speed from that optimization, and we calculate basal melt rates as the sum of the basal frictional heat flux derived from the optimization and the geothermal heat flux from Martos et al. (2017), which was used as input to the optimization. For calculating the basal melt flux from the basal heat flux, we assume the bed is at the pressure melt temperature everywhere, which is a limiting assumption producing the highest melt rates (see Appendix A in Vaňková et al., 2025). Basal melt rates range from a minimum of $\sim 4\,\mathrm{mm\,w.e.\,a^{-1}}$ to a maximum of $> 1\,\mathrm{m\,w.e.\,a^{-1}}$ beneath fast-flowing ice streams in west Antarctica. Basal melting happens everywhere beneath grounded ice in the model, including areas where the bed is likely to be frozen (e.g., Dawson et al., 2022; Seiner et al., 2025). Subglacial drainage model solutions therefore include liquid water in areas that are likely frozen. While the presence of liquid water and the corresponding water pressures may not be realistic for frozen areas, for the purpose of ice-flow modelling, much of the discrepancy can be subsumed into the inferred basal drag coefficient, as long as model results in these regions are interpreted with caution. Implications of the assumption of a thawed bed are discussed in Section 4.4.1.

2.1.3 Steady state and numerics

Simulations are run to a steady state, defined by the rate of change of channel area S and sheet thickness h_s. GlaDS is initialized with zero channel area, sheet thickness 25% of the bed bump height, and water pressure 95% of ice overburden. The perturbed-parameter ensemble pushes GlaDS near its numerical limit, so we impose a soft definition of steady state. For an individual simulation, steady state is defined as 95% of mesh locations having rates of sheet thickness change less than 5% of the bed bump height, $\left|\frac{dh_\mathrm{s}}{dt}\right| \leq 0.0125\,\mathrm{m\,a^{-1}}$, and channel area change less than 5% per year, $\left|\frac{dS}{dt}\right| \leq 0.05 S\,\mathrm{a^{-1}}$. For the ensembles, we continue running all simulations in five-year epochs, including those that are already converged, until these criteria are met for

https://doi.org/10.5194/egusphere-2026-343
Preprint. Discussion started: 3 March 2026

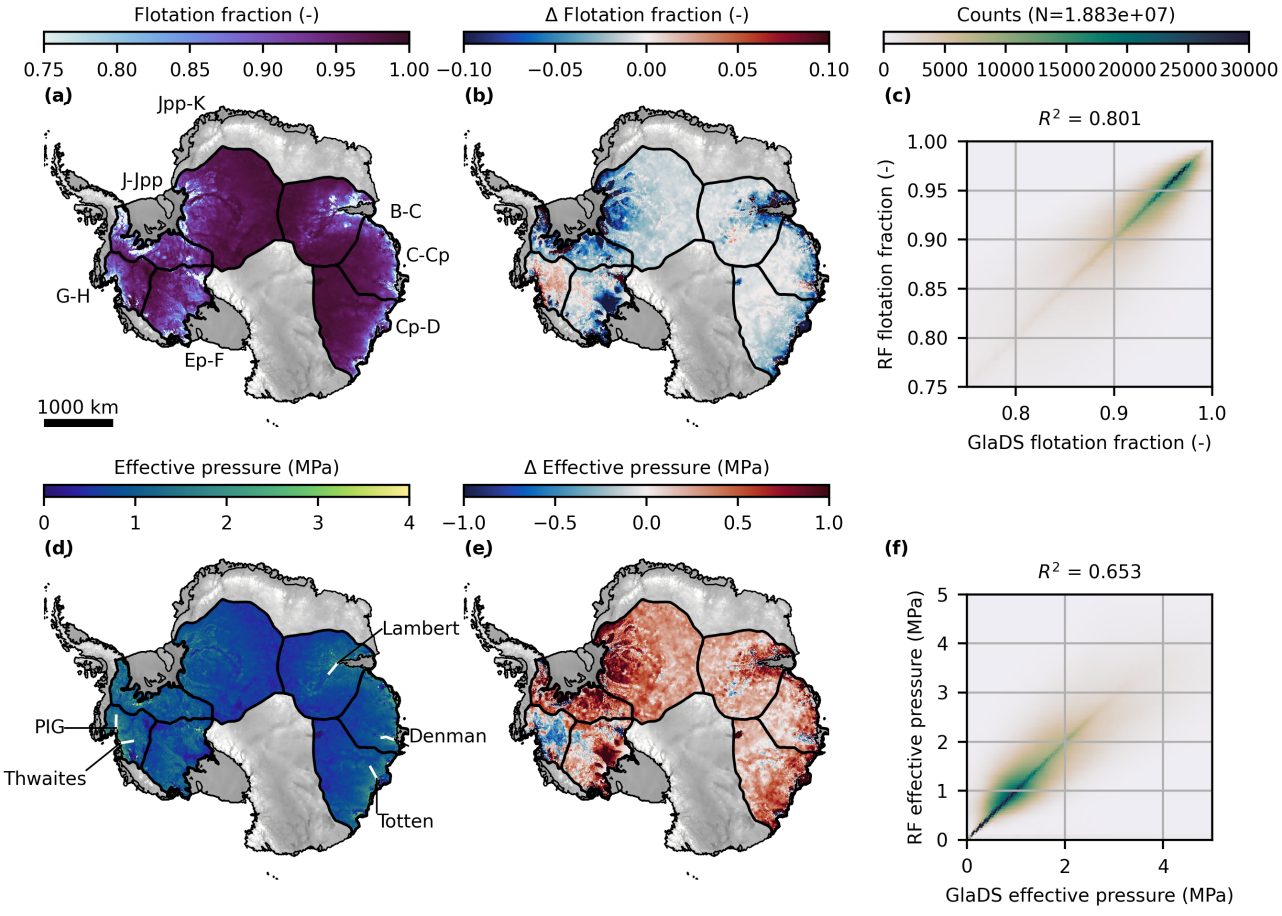

Figure 1. GlaDS simulation outputs and random forest cross-validation prediction error for the median simulation in the ensemble with parameter values $k_s = 0.022\,\mathrm{Pa\,s^{-1}}$, $k_c = 0.077\,\mathrm{m^{\frac{3}{2}}\,s^{-1}}$, $r_b = 42$, $E_{creep} = 0.68$, $l_c = 74\,\mathrm{m}$. (a) GlaDS-simulated flotation fraction and ice-flow basin labels (Rignot et al., 2011b). (b) Random forest cross-validation flotation fraction error. (c) Flotation fraction prediction error for all basins and parameter values. (d) GlaDS-simulated effective pressure and named flowline profiles. (e) Random forest cross-validation effective pressure prediction error. (f) Effective pressure prediction error for all basins and parameter values. Coastlines and grounding lines (Rignot et al., 2011a) are contoured in black. Background map is the BedMachine Antarctica v3 bed elevation (Morlighem et al., 2020).

95% of the simulations. These criteria are met within 10 years in most east Antarctic basins but require 15–30 years in west Antarctica. The Filchner-Ronne basins (J-Jpp and Jpp-K) do not meet these criteria after 30 years, with 93% of simulations converged and very slow rates of convergence in the last 10 years. For the Siple coast (Ep-F), 88% of simulations have met the sheet criterion and only 3% of simulations have met the channel convergence criterion after 30 simulated years and >15 days of walltime per simulation. However, >95% of simulations have $\leq 10\%$ change in sheet thickness and channel area. Based on

https://doi.org/10.5194/egusphere-2026-343
Preprint. Discussion started: 3 March 2026

small rates of improvement over the last five-year epoch, we stop the Siple coast simulations at 30 years, despite the ensemble not reaching the steady state criteria.

The GlaDS governing equations are solved using a numerical residual tolerance (`restol`) of 5×10^{-5}, a maximum of 25 Picard nonlinear iterations, and 10^4 timesteps per year. The $\sim$1 hour timestep, which is short compared to the 2 week timestep used for ice dynamics by Hillebrand et al. (2025b), is necessary for numerical stability given channel flow speeds on the order of meters-per-second and channel segment lengths of $\sim 1\,\mathrm{km}$.

2.2 Experimental design

2.2.1 Training data

We construct training data by running GlaDS on a subset of Antarctic basins (Fig. 1) for present-day conditions. We include three major west Antarctic basins (Amundsen Sea, basin code G-H; Filchner-Ronne ice streams, J-Jpp; and the Siple Coast basin, Ep-F) and four east Antarctic basins (Recovery Ice Stream, Jpp-K; the Amery ice shelf basin, B-C; the Denman Glacier basin, C-Cp; and the Aurora subglacial basin, Cp-D). These basins span a large fraction of the West Antarctic Ice Sheet (WAIS) and the East Antarctic Ice Sheet (EAIS) and include many of the areas that are predicted to undergo the most rapid changes by 2300 (Seroussi et al., 2024).

For each basin, we run an ensemble of 100 GlaDS simulations, perturbing the values of five GlaDS parameters (Table 1). The number of samples is informed by previous work, where 256–512 samples were sufficient for emulating GlaDS as a function of eight parameter values (Hill et al., 2025a, b). We assume that fewer samples are needed for the lower-dimension space sampled here. Parameter values are chosen using a randomized and space-filling Latin hypercube design, a more efficient sampling strategy than full-factorial sampling in five dimensions. Samples are drawn from the logarithm of the parameter values. The lower and upper bounds for parameter values are chosen based on previous modelling and large ensembles (Hill et al., 2025a) combined with heuristic tuning to avoid nonphysical features, such as negative effective pressures over vast swaths of the domain. The bounds for the channel conductivity k_c and bed bump aspect ratio r_b are similar to those used by Hager et al. (2022) and encompass the most commonly used values. The sheet conductivity k_s range used here is not comparable to other Antarctic studies since the units here ($\mathrm{Pa\,s^{-1}}$) differ from the units under the usual turbulent-sheet assumption ($\mathrm{m^{\frac{7}{4}}\,kg^{-\frac{1}{2}}}$). The rate factor for ice deformation, parameterized here by the creep-closure enhancement factor E_creep, is not commonly varied in subglacial drainage modelling studies, despite the high sensitivity to this factor (Hill et al., 2025b) and the uncertainty around ice rheology (e.g., Millstein et al., 2022; Schohn et al., 2025). We vary the sheet-width beneath channels l_c widely around the commonly used value of 2 m (Werder et al., 2013; Pelle et al., 2024).

2.2.2 Future ice-sheet states

To assess how hydrology and ice flow evolve for representative future conditions, we take ice-sheet thickness changes from the Ice Sheet Model Intercomparison Project for CMIP6 (ISMIP6) projections to 2300 from Hillebrand et al. (2025b). Using the reference scenario (`expAE03`) and central parameter estimates, thickness changes from present-day (nominally 2000) to 2050

https://doi.org/10.5194/egusphere-2026-343
Preprint. Discussion started: 3 March 2026

are used for West Antarctica and changes to 2300 for East Antarctica, since these epochs include similar thickness changes for each half of the continent and predate extensive grounding line retreat. By taking snapshots at 2050 (WAIS) and 2300 (EAIS), we bypass the considerable cost of running coupled hydrology–dynamics simulations on centennial timescales. The thickness changes are applied to the BedMachine Antarctica v3 initial condition (Section 2.1.1). Ice is assigned to be floating where the resulting height above flotation is ≤ 0, and the ice shelf base and surface are computed assuming hydrostatic equilibrium, with sea level held fixed at the present-day level. The grounding line is delineated as the boundary between grounded and floating ice. To enable an evaluation of the hydrology parameterization for future ice-sheet states, we run additional GlaDS ensembles using the same parameter sampling strategy as for present-day conditions for the four basins used for ice-flow modelling (Section 2.4). These data are used for evaluation only and are not seen during the training phase.

2.3 Random forest subglacial drainage parameterization

We use a random forest regression model (Breiman, 2001) to parameterize the effective pressure simulated by GlaDS. The random forest learns a pointwise mapping between a vector of features and the simulated GlaDS values, aiming to estimate the GlaDS effective pressure for arbitrary ice-sheet geometries and for various GlaDS parameter values. The random forest is trained on the ensemble of 100 present-day GlaDS simulations in 7 ice-flow basins. The feature vector consists of five GlaDS parameters (Table 1) and nine variables describing the ice-sheet geometry and the forcing fields of the subglacial drainage model (Table 2). In selecting these features, we aim to include a large number and variety of features, anticipating that only a subset will be important for the random forest parameterization. We therefore quantify the importance of each feature and retain only features with non-negligible importance values. Rather than using effective pressure directly, the random forest is trained to predict flotation fraction, the ratio of water pressure to ice overburden pressure, from which the predictions are post-processed to calculate effective pressure. We have found that training the model to predict effective pressure directly has lower generalizability, suggesting that flotation fraction varies more predictably with the geometric characteristics described by the regression features than does effective pressure. Since the random forest is based on pointwise feature and effective pressure values, it does not distinguish between different ice-flow basins and predictions can be made for any region, regardless of whether that region was included in the training data.

The choice of a random forest regression model, rather than other machine-learning models, is based on balancing the ability to learn and generalize from data against training cost and the number of parameters that need to be estimated. Other models, such as a convolutional neural network as used by Verjans and Robel (2024) to emulate Greenland subglacial drainage, would also be appropriate, although a neural network model may be harder to fully integrate within ice-sheet model software than a random forest.

Throughout the investigation of present-day and future subglacial drainage and ice flow, we use the perfect ocean connection assumption (Asay-Davis et al., 2016; Brondex et al., 2019) as a reference point to contextualize and gauge the adherence of

https://doi.org/10.5194/egusphere-2026-343
Preprint. Discussion started: 3 March 2026

Table 2. Complete list of input features considered for the random forest parameterization. The features with the highest permutation-based importance scores are bolded. In all cases, the random forest also makes predictions based on the five GlaDS parameters varied in the ensemble (Table 1).

Features
Bed elevation
Surface elevation
Ice thickness
Distance to grounding line
$\log_{10}$ Basal melt rate
Shreve hydraulic potential
Bed slope
Surface slope
Shreve hydraulic potential gradient

the random forest parameterization to the physics-based model. The perfect ocean connection effective pressure is given by

$$N_{\mathrm{POC}} = \begin{cases} \rho_{\mathrm{i}} g H + \rho_{\mathrm{sw}} g z_{\mathrm{b}}, & z_{\mathrm{b}} \leq 0 \\ \rho_{\mathrm{i}} g H, & z_{\mathrm{b}} > 0 \end{cases}, \tag{1}$$

with ice density ρ_{i}, gravity g, ice thickness H, seawater density ρ_{w}, and bed elevation z_{b} (Table A2).

2.4 Ice-sheet model

Diagnostic velocity solutions using the Ice-sheet and Sea-level System (ISSM) model v4.24 (Larour et al., 2012) are used to evaluate the impact of the effective-pressure parameterization. For simplicity, ice flow is modelled in the four basins considered that do not drain into the Filchner-Ronne or Ross ice shelves (G-H, B-C, C-Cp, Cp-D; Fig. 1). We use the vertically integrated shelfy-stream approximation (SSA) of the momentum balance equations (MacAyeal, 1989) with a nonlinear Budd-type friction parameterization (Budd et al., 1979),

$$\tau_{\mathrm{b}} = C^2 N u_{\mathrm{b}}^{1/p}, \tag{2}$$

for basal drag τ_{b}, spatially varying friction coefficient C, basal slip speed u_{b}, and slip-speed exponent $p = 5$. While a regularized Coulomb friction parameterization may be more justified from physical principles of hard-bed sliding and cavitation (Iken, 1981; Schoof, 2005; Gagliardini et al., 2007) or soft-bed deformation (Zoet and Iverson, 2020), we use nonlinear Budd friction instead to remain consistent with the ice-sheet model runs from which we take the future ice-sheet thickness changes (Hillebrand et al., 2025b). The nonlinearity introduced by $p = 5$ means that the friction coarsely approximates plastic behaviour for fast basal slip while having fewer unconstrained parameters describing unknown bed or cavity characteristics, and only a single

https://doi.org/10.5194/egusphere-2026-343
Preprint. Discussion started: 3 March 2026

unknown parameter at each grid cell to be inferred, compared to a regularized Coulomb relationship (Schoof, 2005; Gagliardini et al., 2007). Several studies have investigated the sensitivity to different forms of the friction parameterization (e.g., Brondex et al., 2019; Åkesson et al., 2021), including with parameterizations for bed weakening near grounding lines (Joughin et al., 2019). We therefore focus on the sensitivity of ice flow to various effective pressure treatments using one representative friction parameterization.

2.4.1 Basal friction inversions

To obtain modelled speeds that are close to present-day observations, we carry out standard control-method inversions (Morlighem et al., 2010) for the spatially varying friction coefficient C using InSAR-derived surface velocity (Rignot et al., 2011b, 2017). We perform the inversion using present-day geometry independently for each of three effective pressure scenarios (GlaDS, random forest (RF), perfect ocean connection (POC)) to obtain three friction fields (C_{GlaDS}, C_{RF}, and C_{POC}). An alternative approach would be to carry out a single inversion for basal drag. From this reference inversion, the friction coefficients for each effective pressure field could be calculated to obtain identical basal drag fields in each scenario (e.g., Brondex et al., 2019). We choose to perform independent inversions as a more fair assessment of what would be obtained in realistic modelling scenarios that choose a particular effective pressure field, with differences in the inferred friction coefficient between these approaches only being due to regularization. For the future scenarios presented in Section 3.5.2, these friction fields are held constant in time and are used with the effective pressure fields representing future conditions to compute future ice-flow speeds. In the case of GlaDS and random forest effective pressures, we use the mean effective pressure from the perturbed-parameter ensembles. To compute ice-flow solutions for each of the 100 ensemble members, we algebraically rescale the friction coefficient C based on the ratio of the effective pressure to the ensemble-mean value that is used in the friction inversions as described in the alternative approach above, rather than carrying out 100 independent inversions. Inversions use absolute and log-misfit cost functions combined with a regularization term penalizing large friction coefficient gradients (Eq. B2). The weights for the regularization term are determined by L-curve analysis (Fig. B1).

3 Results

3.1 Subglacial drainage model ensemble

Since random forest predictions will be poor when extrapolating outside the training range of GlaDS parameters, we first explore the behaviours seen in the GlaDS ensemble and evaluate whether the ensemble represents what might be considered realistic drainage systems. For most major outlet glaciers with published subglacial drainage model results, the proportion of channelized drainage in the GlaDS ensembles brackets that reported elsewhere (Fig. A1, Table A1). The ensemble mode of grounding-line channelized discharge is close to published values in east Antarctica, but it is biased towards lower channel discharge for Thwaites and Pine Island. Differences in all regions may partly be a function of the laminar–turbulent sheet-flux parameterization used in the GlaDS simulations (Hill et al., 2024) and the assumption of a temperate bed that was made to

https://doi.org/10.5194/egusphere-2026-343
Preprint. Discussion started: 3 March 2026

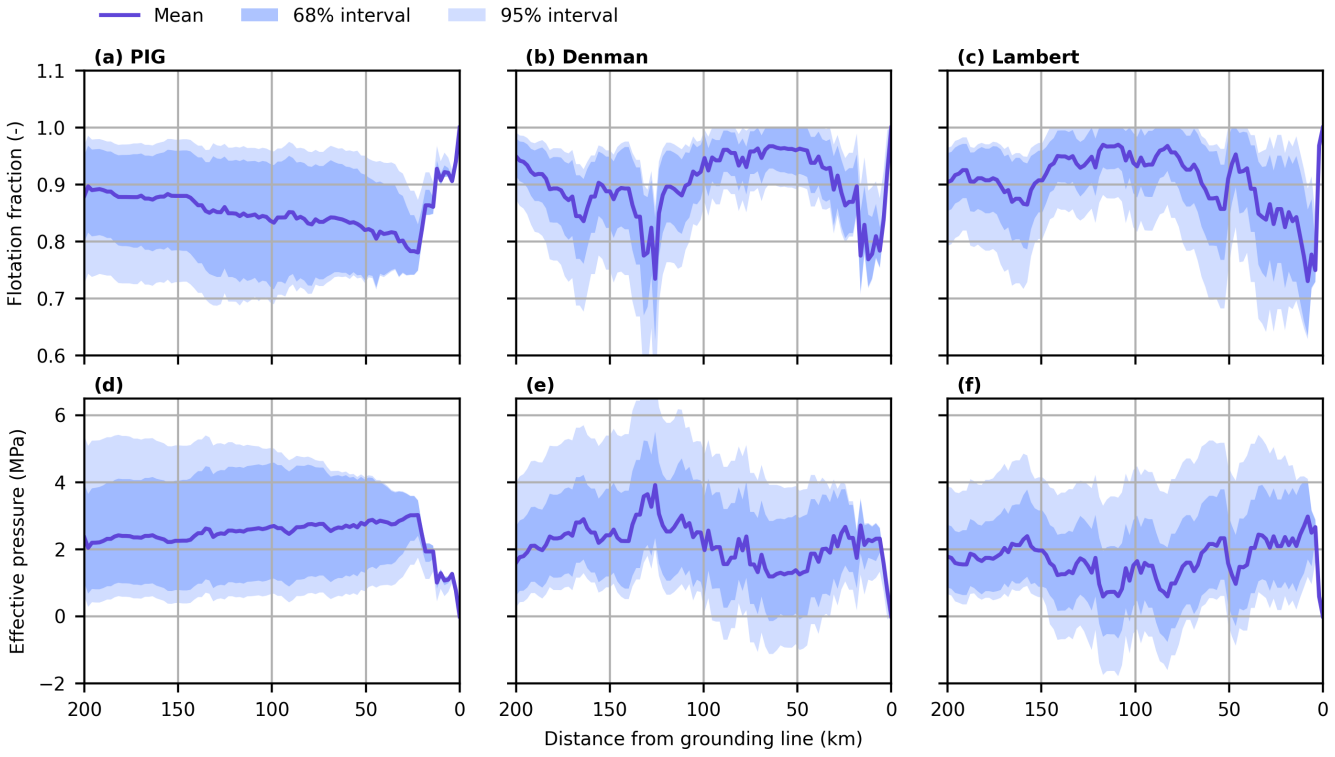

Figure 2. Profiles of flotatio language=en n fraction (top row) and effective pressure (bottom row) for selected outlet glaciers from the ensemble of 100 GlaDS simulations. Shaded areas indicate the range of the central 68% (approximately one standard deviation around the median) and 95% (approximately two standard deviations around the median) of the ensemble members. The solid line indicates the ensemble mean. Outlet glaciers are labelled in Fig. 1(d).

compute the basal melt-rate field (Section 2.1.2), which results in larger total meltwater volumes, and therefore higher channel discharge, in east Antarctica than if parts of the bed are frozen.

The spatially distributed flotation fraction and effective pressure vary strongly across the ensemble. Flotation fraction varies between ∼60–105% for the central 95% of simulations (Fig. 1a–c). The spread of effective pressure across the central 95% of the ensemble is comparable to or greater than the mean, such that there is a ≥100% spread in the modelled effective pressure (Fig. 1d–f). For instance, at Pine Island Glacier, we see GlaDS simulations with effective pressure consistently below 1 MPa and other simulations with effective pressure above 4 MPa (Fig. 2(d)). Flotation fraction and effective pressure show a narrower spread within ∼ 10 km of the grounding line, as expected given the flotation boundary condition and reduced ice thicknesses near the grounding line. The wide spread of flotation fraction, effective pressure, and channelized grounding-line discharge suggest that the perturbed-parameter ensemble covers a wide range of drainage-system configurations and brackets our prior assumptions of what constitutes a realistic drainage system. Therefore, end-users of the parameterization are unlikely to need to extrapolate outside of the training space.

https://doi.org/10.5194/egusphere-2026-343
Preprint. Discussion started: 3 March 2026

3.2 Model sensitivity

To better understand characteristics of the random forest parameterization and guide the settings and data used for training the final model, we assess the sensitivity of the random forest model to the features used for prediction and the basins used for training. This sensitivity analysis uses a random forest model trained on only the mean of the 100 perturbed-parameter simulations for computational reasons and to isolate the role of the geometric features. The ensemble-mean random forest is evaluated in Table C1. The accuracy of the random forest parameterization is quantified by the coefficient of variation R^2 that measures the proportion of variance of the GlaDS model outputs that is captured by the random forest parameterization. Values are usually between 0 and 1, with $R^2 = 0$ indicating a poor fit with none of the GlaDS variations captured by the predictions, and $R^2 = 1$ indicating that the predictions match the GlaDS values perfectly. Negative R^2 values are possible and indicate that the predictions have greater residuals than would be obtained by using the spatially uniform mean of the simulations as a prediction.

3.2.1 Feature importance

We identify the most and least important features in order to simplify the random forest parameterization. Feature importance is quantified using a permutation-based metric (Breiman, 2001) that measures the decrease in R^2 for predictions where the values of one feature are randomly shuffled (Fig. 3). Based on the importance scores, the random forest strongly relies on ice thickness for predictions of both flotation fraction and effective pressure. Randomly shuffling the ice thickness values leads to a mean decrease in R^2 of 1.8 for the flotation fraction field and 18 for effective pressure. The surface elevation, bed slope, and Shreve potential slope have a negligible impact on random forest predictions. The random forest has some sensitivity to the remaining features, but their influence is small compared to that of ice thickness. Based on these feature-importance rankings, we fit a simpler model based on the four most important features: ice thickness, bed elevation, Shreve potential and surface slope. The decision to exclude the grounding-line distance and basal melt rate (the fifth and sixth most important features) is based on their lower feature importance values, as well as the fact that they are not directly extractable from ice-sheet model inputs. Excluding these features makes the random forest parameterization easier to use and not meaningfully less accurate. We do not find differences in the relative importance of the four features for the retrained reduced model (Fig. 3(b)). Manually inspecting the tree structures (Fig. D1) and computing Shapely Additive exPlanation (SHAP) (Lundberg and Lee, 2017) values (Fig. D2) further support the importance of ice thickness.

3.2.2 Influence of the basins used for training

To assess whether predictions are disproportionately sensitive to any particular basin, we retrain the ensemble-mean random forest after removing training data from each basin individually and repeat the cross-validation exercise. The sensitivity is quantified by the difference in R^2 between these new and original cross-validation predictions (Fig. 4(a)). The strongest sensitivity is found for Recovery basin (Jpp-K), which has improvements of $\Delta R^2 = 0.12$ when excluding each of the Amundsen sea (G-H) or western Filchner-Ronne (J-Jpp) basins, suggesting conditions are different in the Recovery basin than these other

https://doi.org/10.5194/egusphere-2026-343
Preprint. Discussion started: 3 March 2026

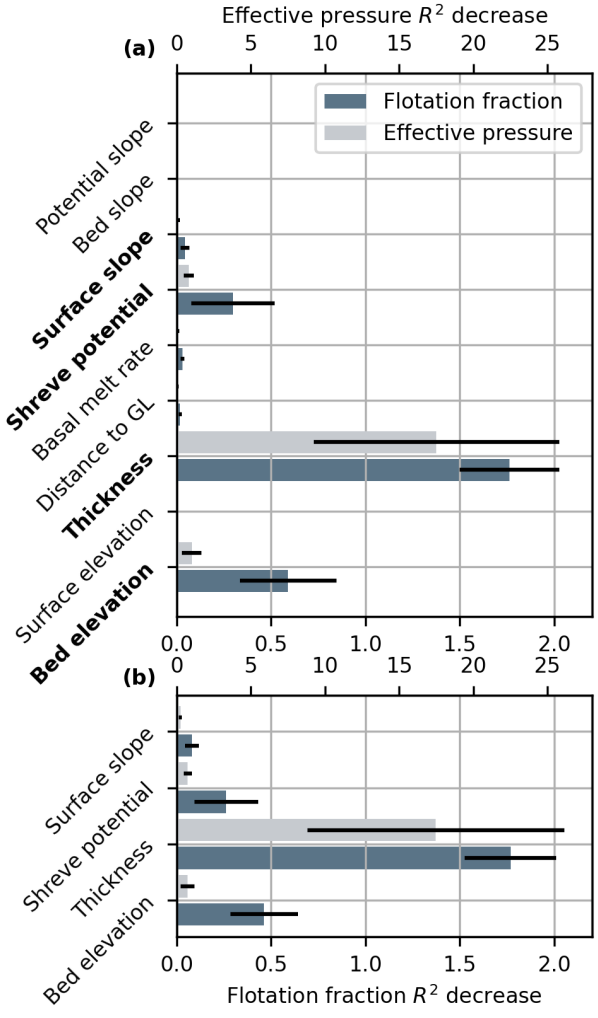

Figure 3. Permutation-based feature importance when predictions are in flotation fraction (bottom abscissa) and effective pressure units (top abscissa) when using all prediction features (a) and for the simplified model that depends on only the four most important features (b). Bolded labels in (a) indicate the features used in (b).

west Antarctic basins. For other basins, predictions are sometimes worsened when nearby basins are excluded, suggesting similar conditions across ice divides. For instance, Siple coast (Ep-F) predictions are made slightly worse when excluding the western Filchner-Ronne basin (J-Jpp) with $\Delta R^2 = -0.07$, and Aurora basin (Cp-D) and the Denman basin (C-Cp) are mutually dependent with $\Delta R^2 = -0.05$.

To assess the relationship between the quantity of training data and the performance of the random forest, we retrain the random forest taking subsets of the training data. For all possible subsets of 2–7 basins, we retrain the random forest while additionally excluding the test basin from training (training uses 1–6 basins) (Fig. 4(b)). For all basins, the change in R^2

https://doi.org/10.5194/egusphere-2026-343
Preprint. Discussion started: 3 March 2026

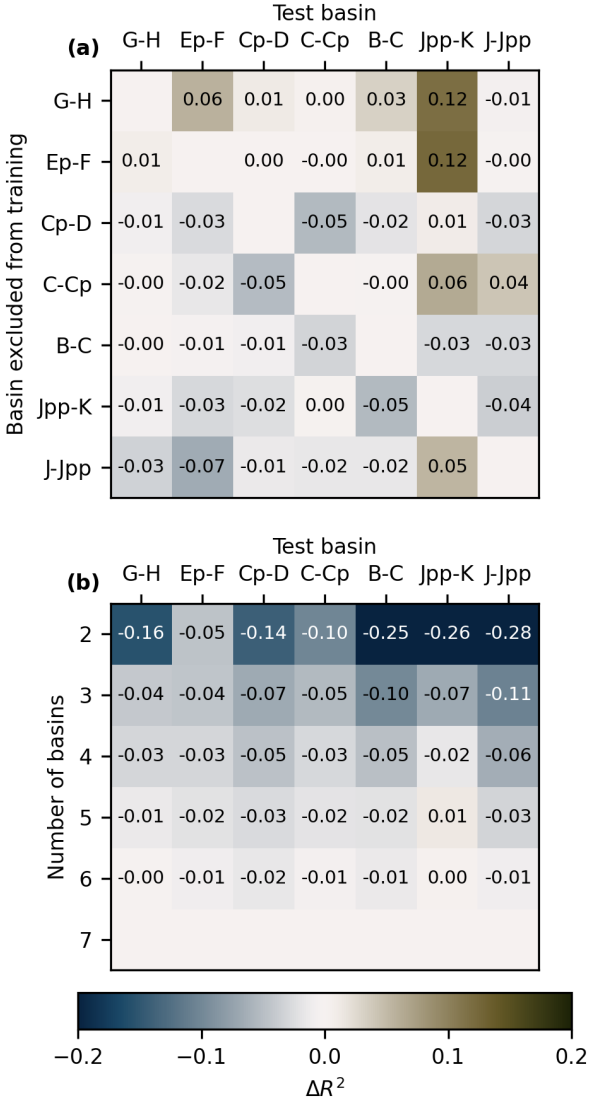

Figure 4. Sensitivity to the basins used for training. (a) Change in R^2 relative to the original cross-validation predictions when removing individual training basins. (b) Average change in R^2 relative to the original cross-validation predictions when retrained with all possible combinations of different numbers of basins.

is small ($|\Delta R^2| \leq 0.03$) when including 5–6 basins compared to the original cross-validation predictions. Predictions are worsened when including only 2–3 basins. For instance, we find that the predictions for the Filchner-Ronne basins (J-Jpp, Jpp-K) have an R^2 that is lower by 0.26–0.28 on average when using only one other basin for training compared to the original cross-validation predictions. These results suggest that 4–5 basins are sufficient for training the random forest.

https://doi.org/10.5194/egusphere-2026-343
Preprint. Discussion started: 3 March 2026

Table 3. Cross-validation evaluation of the random forest model. Coefficient of variation R^2 values are computed using GlaDS simulated values as the reference. Values are presented for predictions expressed in flotation fraction (f_w) and effective pressure (N) units and for the entire domain ("All"), where surface speed $u > 200\,\mathrm{m\,a^{-1}}$, and for the whole domain after interpolation onto a regular grid with resolution 2.5 km ("Gridded"). Flow speed u is evaluated by using the random forest cross-validation predictions in place of the GlaDS effective pressure, using the friction coefficient inferred with GlaDS effective pressure. Speed results are reported only for the four basins used for ice-flow modelling (see Section 3.5.1).

	f_w			N			u
Basin	All	$u > 200\,\mathrm{m\,a^{-1}}$	Gridded	All	$u > 200\,\mathrm{m\,a^{-1}}$	Gridded	Present-day
Amundsen Sea (G-H)	0.83	0.74	0.81	0.69	0.71	0.58	0.996
Amery (B-C)	0.85	0.80	0.86	0.74	0.69	0.74	0.99
Denman (C-Cp)	0.82	0.90	0.83	0.67	0.80	0.69	0.98
Aurora (Cp-D)	0.82	0.85	0.82	0.72	0.83	0.73	0.94
Recovery (Jpp-K)	0.79	0.83	0.77	0.67	0.70	0.65	N/A
Siple Coast (Ep-F)	0.76	0.76	0.65	0.65	0.78	0.42	N/A
Filchner-Ronne (J-Jpp)	0.81	0.83	0.76	0.67	0.82	0.55	N/A
Overall	0.80	0.79	0.79	0.65	0.77	0.61	0.99

3.3 Evaluation of the random forest parameterization

3.3.1 Accuracy of the parameterization

Aggregated across the seven basins and cross-validated parameter values, the random forest explains 80% (range: $R^2 = 0.76$–0.85) of the variance of the GlaDS simulated flotation fraction outputs. Performance reduces to $R^2 = 0.65$ in effective pressure N units (range: $R^2 = 0.65$–0.74; Table 3). The reduced performance when evaluated in effective pressure units is consistent with previous findings (Hill et al., 2025a), supporting that it is more challenging to predict effective pressure than flotation fraction. This should be expected since pressures are near flotation. A small change in flotation fraction translates into a large relative change in N. For instance, with a flotation fraction of 90%, a 1% error translates to a 10% relative error in effective pressure. The performance of the random forest in units of hydraulic potential ($R^2 = 0.988$) is comparable to the CNN emulator developed by Verjans and Robel (2024) to reproduce hydraulic potential for Greenland outlet glaciers ($R^2 = 0.96$).

Motivated by the amplified importance of subglacial hydrology in fast-flowing regions, we compute R^2 values for the random forest predictions where surface speeds are $> 200\,\mathrm{m\,a^{-1}}$, finding that R^2 values for effective pressure are higher in fast-flowing areas than for the domain as a whole except for the Amery ice shelf basin (B-C). The improvement is most pronounced for the Siple coast (Ep-F), which improves from $R^2 = 0.65$ to 0.78 when focusing on fast-flowing areas. To assess how the uneven weighting of the variable resolution meshes influences the performance metrics, we regrid the predictions onto a square mesh with uniform $2.5\,\mathrm{km}$ resolution ("Gridded" columns in Table 3). Basins with complex or unusual geometry in slow-flowing

https://doi.org/10.5194/egusphere-2026-343
Preprint. Discussion started: 3 March 2026

Table 4. Coefficient of variation (R^2) values for the random forest parameterized flotation fraction (f_w), effective pressure (N), and resulting surface speed (u) for representative future ice-sheet states in the four basins with future GlaDS ensembles and ice-flow results.

Basin	Year	f_w	N	u
Amundsen (G-H)	2050	0.89	0.86	0.998
Amery (B-C)	2300	0.88	0.83	0.98
Denman (C-Cp)	2300	0.86	0.72	0.98
Aurora (Cp-D)	2300	0.88	0.84	0.96
Overall	N/A	0.88	0.82	0.99

areas with coarse mesh resolution, such as Siple dome (basin Ep-F), high-elevation plateaus along the Filchner-Ronne coast (Jpp-K, J-Jpp), and subglacial volcanoes in the Amundsen sea (G-H) have lower R^2 values after gridding since errors associated these features are weighted more heavily. Other basins with errors mostly occurring where the mesh is refined near the coast, such as Denman (C-Cp) and Aurora (Cp-D) basins have a slightly higher R^2 value after gridding since these areas are given less weight.

3.4 Projected changes in effective pressure

Using the GlaDS simulations for future ice-sheet configurations, we assess how faithfully the random forest parameterization, which is trained on present-day conditions, predicts flotation fraction and effective pressure at 2050 (WAIS) and 2300 (EAIS) relative to steady-state GlaDS simulations (Table 4). Based on the higher R^2 values, random forest predictions for the perturbed geometries, representing 2050 and 2300, are better than the cross-validation predictions for present day (Table 3).

By predicting continent-wide effective pressure at 2300 using the random forest parameterization, we find a pattern of drastic reductions in effective pressure coincident with the largest thickness changes (Fig. 5). We also find a slight stabilizing influence where effective pressure increases relative to present day immediately upstream of grounding lines as they retreat. This effective pressure increase occurs despite. these areas having undergone hundreds of meters of thinning that would usually act to reduce effective pressure. The increase in effective pressure is most pronounced for Totten Glacier, the West Ice Shelf area, Cook Glacier in the Wilkes subglacial basin, the remnants of WAIS, and on the southern and eastern boundary of the Filchner-Ronne Ice Shelf (Fig. 5d).

3.5 Impact on ice flow

As the motivation for the random forest parameterization is to facilitate the inclusion of active subglacial drainage in ice-sheet models, we evaluate the sensitivity of ice flow to substituting the random forest parameterization for the physics-based drainage model. We investigate the sensitivity of both present-day and future modelled ice flow to the parameterization of

https://doi.org/10.5194/egusphere-2026-343
Preprint. Discussion started: 3 March 2026

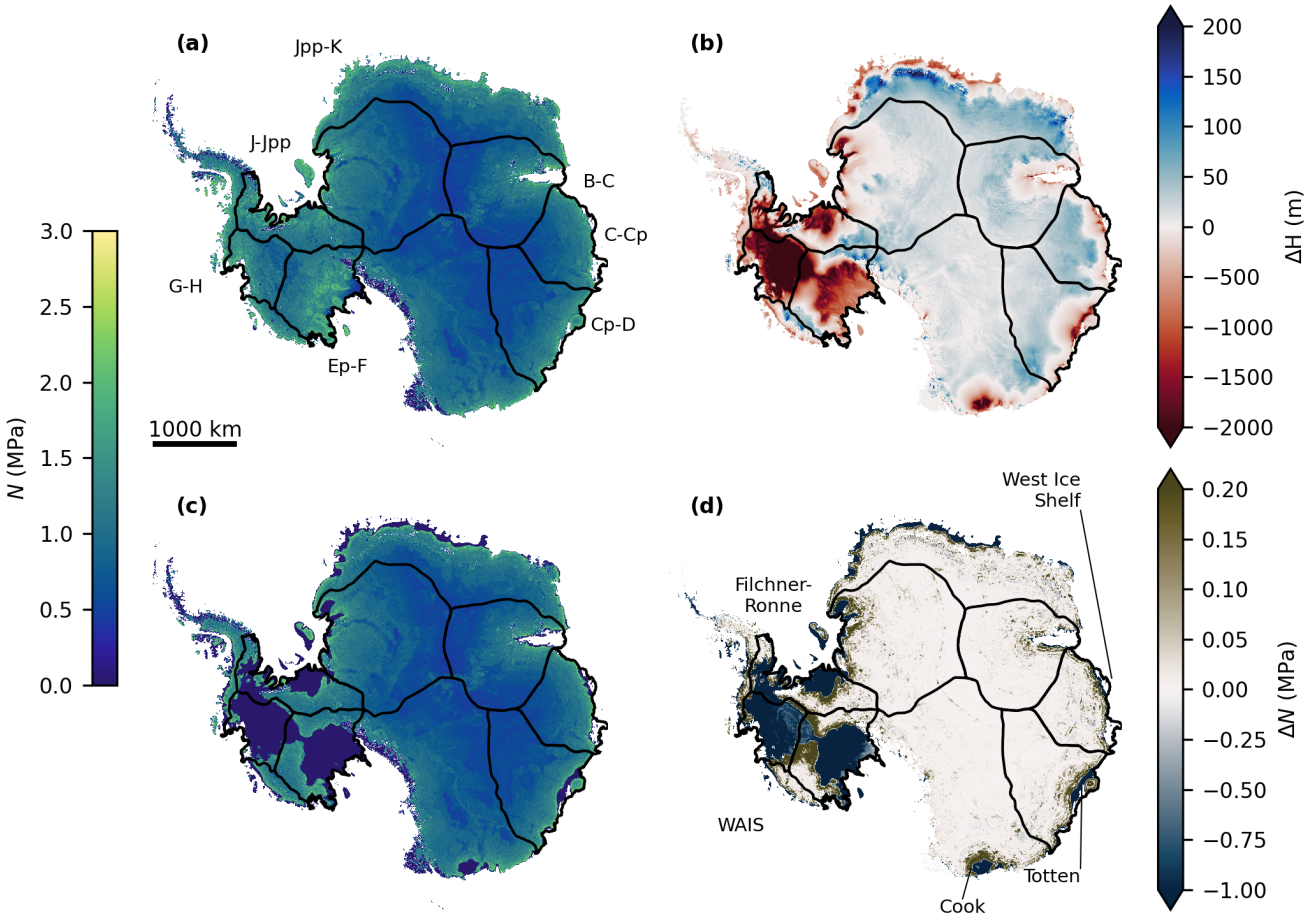

Figure 5. Continent-wide random forest effective pressure (N) predictions for present-day and future geometries for the median simulation (parameter values listed in Fig. 1 caption). (a) Random forest N prediction for present-day geometry. Black lines and text labels delineate the present-day ice-flow basins used for training. (b) Thickness change from 2000 to 2300 (Hillebrand et al., 2025b). (c) Random forest N prediction for 2300 geometry. Areas with zero effective pressure at 2300 indicate areas where grounded ice has been completely removed. (d) Difference in effective pressure from present-day to 2300. Labels correspond to regions discussed in the text. Note the asymmetric colour scales in (b) and (d).

subglacial effective pressure using diagnostic ice-sheet solutions that solve for ice velocity using prescribed geometry and various effective pressure treatments in the basal friction parameterization.

https://doi.org/10.5194/egusphere-2026-343
Preprint. Discussion started: 3 March 2026

3.5.1 Present-day ice flow

Starting with present-day geometry, we separately carry out control-method inversions for basal friction fields (Appendix B) using effective pressure fields from the perfect-ocean-connection assumption (N_{POC}, resulting in friction coefficient C_{POC}), GlaDS (N_{GlaDS}, C_{GlaDS}) and the random forest parameterization (N_{RF}, C_{RF}). With the friction coefficient inferred to match observed surface speeds, both GlaDS and Random-forest-parameterized N fields produce nearly identical fits to the observed surface speed when using corresponding friction and effective pressure fields, as evidenced by the close fit between $C_{\mathrm{GlaDS}}/N_{\mathrm{GlaDS}}$ and $C_{\mathrm{RF}}/N_{\mathrm{RF}}$ speed profiles (Fig. 6c). This scenario serves to validate the model setup and illustrate that, for present-day conditions, the basal friction inversion compensates for differences in effective pressure.

To assess how differences in the effective pressure fields propagate into differences in ice flow, we change the effective pressure used for the forward velocity solution while holding the friction coefficient constant as C_{GlaDS}. Using the random forest effective pressure with GlaDS friction coefficient ($C_{\mathrm{GlaDS}}/N_{\mathrm{RF}}$) results in $R^2 = 0.99$ between the speed fields (Table 3), showing that ice flow responds less strongly to the substitution of the emulated effective pressure than suggested by the domain-wide $R^2 = 0.65$ between simulated and emulated effective pressure. Using the perfect ocean connection effective pressure for the forward velocity solve ($C_{\mathrm{GlaDS}}/N_{\mathrm{POC}}$) closely reproduces speeds near the grounding line, where the ocean-connection parameterization is appropriate. The perfect ocean connection parameterization breaks down inland of the grounding line, resulting in significantly slower ice flow. Since the inferred friction coefficient compensates for differences in effective pressure when varying the parameters of the subglacial drainage model, the results in Fig. 6, presented for the ensemble mean, should be qualitatively similar for other ensemble members. While it is an unrealistic modelling setup to use a different effective pressure field for solving the forward model than was used in the friction inversion, this experiment isolates the sensitivity of ice flow to the treatment of effective pressure.

3.5.2 Future ice flow

Holding the present-day friction-coefficient fields constant in time, we solve for velocity given the imposed thinning at 2050 (WAIS) and 2300 (EAIS). Velocity solutions are computed separately for GlaDS, random forest and perfect ocean connection effective pressure fields while using the corresponding friction coefficient inferred from present-day conditions and surface velocity observations. For each effective pressure model, we include an additional scenario that isolates the role of changes in N from changes in geometry by carrying forward the present-day N field and comparing against the corresponding scenario with evolving N.

Modelled speeds are sensitive to the choice of effective pressure model (Fig. 7). At the grounding line, the range in speed among all N models varies from $441\,\mathrm{m\,a^{-1}}$ (PIG) to $2199\,\mathrm{m\,a^{-1}}$ (Lambert). Taking speeds obtained by driving the ice-sheet model with the future GlaDS effective pressure as the reference, the relative difference in grounding-line speed between the low and high end-members is between 8.5% (PIG) and 251% (Totten). Taking grounding-line speed as a proxy for dynamic ice discharge, these differences imply there could be divergent rates of ice-sheet evolution and sea-level contributions predicted between these effective pressure scenarios. The highest speeds are consistently predicted by the perfect ocean connection

https://doi.org/10.5194/egusphere-2026-343
Preprint. Discussion started: 3 March 2026

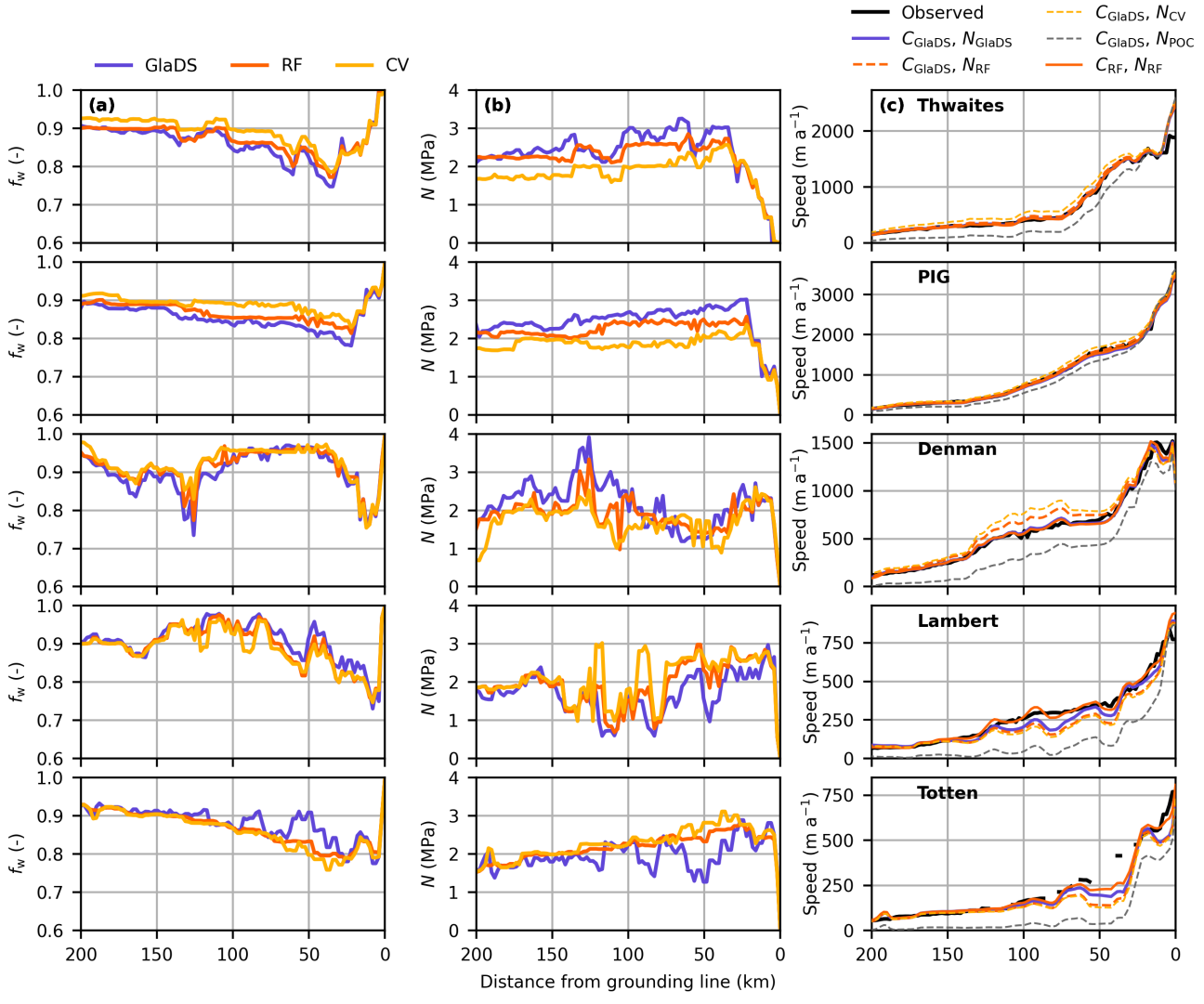

Figure 6. Comparison of present-day hydrology and ice-flow variables for the named flowlines shown in Fig. 1(d). (column a) Ensemble-mean flotation fraction from GlaDS and from the random forest when trained on the entire dataset (RF), as well as for the cross-validation predictions (CV). (column b) As in column (a) but for effective pressure. (column c) Depth-averaged flow speed for various combinations of the GlaDS and random forest friction coefficient and the GlaDS, random forest and perfect ocean connection effective pressure. Gaps in the observed velocity field for Totten Glacier (bottom right panel) correspond to incomplete spatial coverage in the InSAR-derived ice-flow map (Rignot et al., 2011b).

effective pressure field, and the lowest speeds correspond to an effective pressure that does not change in time (i.e., speed changes are caused by change in ice thickness only, as is the case for projections with static basal friction). Using modelled

https://doi.org/10.5194/egusphere-2026-343
Preprint. Discussion started: 3 March 2026

effective pressure that responds to changes in ice thickness, either with GlaDS or the random forest parameterization, results in a speed bounded between these two end-members.

Using the random forest effective pressure reproduces modelled future ice speeds with $R^2 = 0.99$ relative to the reference scenario using GlaDS (Table 4). For the major outlet glaciers labelled in Fig. 1(d), the random forest has grounding-line speed differences of $78\,\mathrm{m\,a^{-1}}$ (Totten) to $311\,\mathrm{m\,a^{-1}}$ (Lambert), or 2.1% (PIG) to 10% (Denman) relative to the future GlaDS scenario (Table C3). In all basins, the random forest parameterization results in the closest match to the velocities using GlaDS directly. For the random forest trained on the ensemble-mean, the difference reduces to 0.6–6.7% of the reference speed (Fig. C1), excluding Totten which has an unconstrained friction coefficient in the region of the retreated grounding line.

3.5.3 Effect of subglacial hydrology parameters on ice dynamics

To assess the role of uncertainty in subglacial hydrology parameter values, we solve for ice velocities at 2050 (WAIS) and 2300 (EAIS) for each of the 100 perturbed-parameter simulations. The resulting grounding-line speed spans nearly the entire range between the slow (static effective pressure) and fast (ocean connection effective pressure) end-members, highlighting the importance of parameter uncertainty (Fig. 7c). Counter-intuitively, the highest speeds correspond to high effective pressures, related to small creep-enhancement factors $E_{\mathrm{creep}} < 1$ and high sheet k_{s} and channel k_{c} conductivities. The lowest speeds are related to low effective pressure resulting from high creep-enhancement factors $E_{\mathrm{creep}} > 1$. The fact that high speeds are obtained with high effective pressure, and vice versa, is related to the compensation of the friction coefficient inversion. By design, the friction coefficient ensures that present-day speeds are matched for all parameter values. The speeds for the perturbed geometries depend on the change in effective pressure relative to the initial state used in the friction inversion. Parameter values that result in the highest effective pressure also result in the largest change near the grounding line as the grounding line retreats, bringing with them the largest reduction in basal drag and largest speed up. Simulations with very low effective pressure show almost no change as the grounding line retreats. Subglacial hydrology does not contribute to changes in basal drag for these ensemble members, resulting in the lowest speeds. Using the random forest parameterization instead of GlaDS recovers a similar range of grounding-line speeds and the same conclusions about the role of parameter uncertainty.

3.6 Computational savings

GlaDS simulations take ∼16–97 hours to run per five-year epoch on a single AMD EPYC 7532 CPU, with total runtimes between 32–388 hours to reach steady state as defined in Section 2.1.3. Training the random forest takes 124 seconds, predictions on each basin take 0.28–0.52 seconds, and continent-wide predictions at 2 km resolution take ∼21 seconds. Depending on the basin, predictions with the trained random forest are therefore 10^5–$10^6\times$ faster than the numerical model simulations, and the one-time training cost is negligible compared to the cost of generating the training data. The cost of random forest predictions scales nearly linearly with respect to the number of prediction locations and the random forest is trivially parallelizable since predictions only use local information.

The random forest parameterization addresses only one aspect of the cost of coupled hydrology and dynamics simulations. The ice flow simulations presented here take ∼10 seconds per basin on a single CPU. Continent-wide, higher-order ice-flow

https://doi.org/10.5194/egusphere-2026-343
Preprint. Discussion started: 3 March 2026

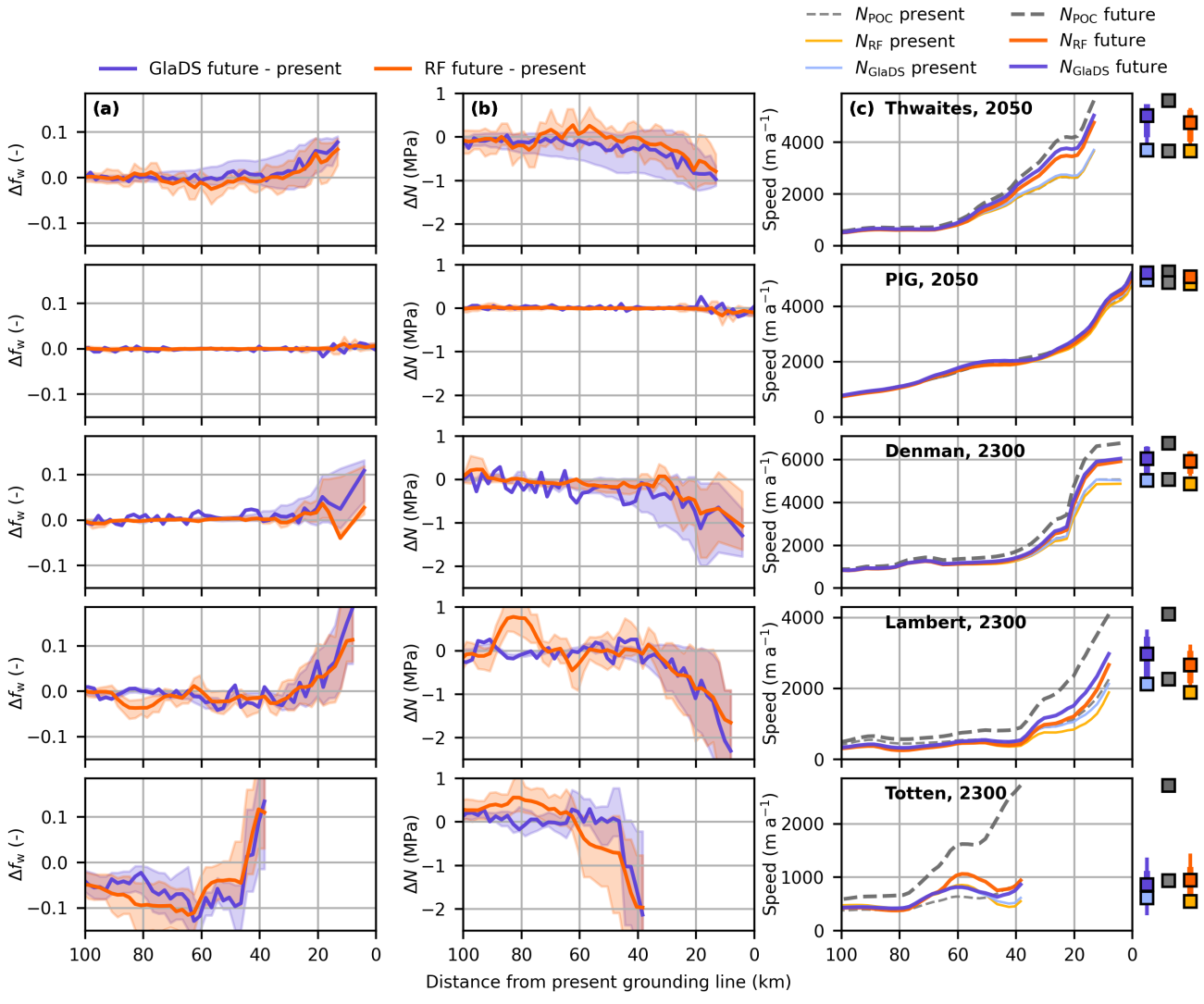

Figure 7. Sensitivity of ice speed to effective pressure for representative future ice-sheet geometries. (column a) Flotation fraction difference from present day and (column b) effective pressure difference from present day simulated by GlaDS and predicted by the random forest (RF). Shaded areas indicate the central 68% of values. (column c) Modelled speed corresponding to present-day and future GlaDS, random forest (RF) and perfect ocean connection (POC) effective pressure fields. Square markers to the right of column (c) indicate the speed at the grounding line for the corresponding effective pressure fields. The vertical bars indicate the spread of the central 68% (thick line) and 95% (thin line) speeds from the 100 perturbed-parameter samples simulated by GlaDS and predicted by the random forest parameterization. Refer to Fig. 1(d) for flowline locations. Flowlines are truncated at the retreated grounding line.

models and transient simulations will be more resource-intensive than the simple SSA model used here. While we have not reduced these costs, we have eliminated the significant bottleneck of the hydrology model.

https://doi.org/10.5194/egusphere-2026-343
Preprint. Discussion started: 3 March 2026

4 Discussion

4.1 Sensitivity of ice flow to effective pressure

For present-day conditions, we show that modelled speed is weakly sensitive to substituting the random forest in place of GlaDS, relative to the differences in effective pressure fields themselves, even while using the same friction coefficient for both stress-balance solutions (Fig. 6, Table 3). Given the action of ice flow as a low-pass filter with a threshold of several ice thicknesses (Kamb and Echelmeyer, 1986), the response of ice flow to any difference in effective pressure on shorter length scales will be strongly damped. Errors in effective pressure where ice flow is slow or where basal drag is a minor component of the stress balance will also not be strongly reflected in observed ice flow.

For perturbed geometries representative of plausible future conditions, there is a consistent hierarchy in ice-flow speeds based on how effective pressure is determined. Using the perfect ocean connection model for effective pressure overestimates future speeds relative to using the physics-based model, and holding effective pressure fields constant in time while the ice-sheet thickness changes underestimates speed. The random forest is the closest match to re-running GlaDS to steady-state using the perturbed geometry in all basins. This hierarchy of speeds is consistent with studies comparing Weertman friction, which is mathematically analogous to Budd friction with constant effective pressure, to Budd friction with parameterized effective pressure. For instance, Åkesson et al. (2021) project for 2300 that terminus speeds for Petermann Glacier, Greenland, are $1500\,\mathrm{m\,a^{-1}}$ with a Weertman (i.e., static effective pressure) friction parameterization and $> 2000\,\mathrm{m\,a^{-1}}$ with a Budd parameterization using perfect ocean connection effective pressure. For the Amundsen Sea basin, Brondex et al. (2019) show that the largest ice mass loss by 2100 corresponds to Budd friction assuming ocean connectivity, compared to Weertman and regularized Coulomb friction parameterizations. Ma et al. (2025) find greater grounding line retreat for Totten glacier at 2100 when the perfect ocean connection assumption is used compared to assuming effective pressure is everywhere 5% of ice overburden. Zhao et al. (2025) show that using static, present-day GlaDS effective pressure, which is analogous to Weertman friction, results in the lowest grounding-line flux and the smallest sea-level contribution from Antarctica by 2300 among the scenarios that they consider, with some differences related to the form of the friction parameterization. When effective pressure is parameterized to decrease near the moving grounding line, either through height-above-flotation scaling of the friction coefficient (Joughin et al., 2010) or modelling effective pressure with the perfect ocean connection assumption, the grounding-line flux increases, resulting in larger sea-level contributions. To these findings, we add that the subglacial drainage model can reproduce these end-members for extreme parameter values.

Consistent with other studies (Pelle et al., 2023, 2024; Zhao et al., 2025), we find that the sensitivity of ice flow to effective pressure varies between glaciers. For instance, we find very little difference in modelled speed when using different effective pressures with the same friction coefficient for present-day Pine Island Glacier compared to its neighbour Thwaites (e.g., CV vs. GlaDS effective pressure in Fig. 6c). These differences may reflect differing stress-balance regimes, where the relative influence of buttressing, lateral shear, longitudinal stress coupling, and basal drag vary on a glacier-specific basis. For Pine Island, this suggests that basal drag may not be a dominant term in its stress balance. In the case of the future ice-sheet experiments, the minimal change in velocity relative to present day for Pine Island Glacier can be explained by the imposed

https://doi.org/10.5194/egusphere-2026-343
Preprint. Discussion started: 3 March 2026

thickness changes (Sec. 2.2.2) for Pine Island Glacier at 2050 being very small. This is related to those imposed thickness changes being derived from simulations with a calibration of the ice-shelf basal melt flux for Pine Island and Thwaites glaciers as a single region (Jourdain et al., 2020; Hillebrand et al., 2025b). This results in an underestimation of melting near the Pine Island Ice Shelf grounding line, and, therefore, a likely underestimation of the future thinning rate of grounded ice and corresponding effective-pressure changes.

The large spread in modelled speeds for future geometries indicates there would be different paces of ice-sheet evolution predicted between these scenarios. Based on modelled grounding-line speeds, perfect ocean connection effective pressure may result in the earliest onset of unstable marine ice-sheet retreat, while keeping effective pressure constant would delay the onset. Pelle et al. (2024) suggest that hydrologic feedbacks accelerate retreat of Totten Glacier by 25 years (2035 vs. 2060) through ice-shelf melt feedbacks, with very minor impacts related to changes in basal friction relative to a baseline scenario using perfect ocean connectivity. The fact that ocean-connection effective pressure overestimates speeds in our simulations suggests that experiments using ocean connectivity as the baseline, such as in Pelle et al. (2024), may understate the role of hydrology in controlling ice-sheet retreat and mass loss through reductions in basal drag.

4.2 Influence of subglacial drainage model parameters

Several parameters of the GlaDS model have large uncertainty. Calibrating the model with direct measurements such as borehole water pressure has proven to be challenging and provides only moderate constraints on plausible parameter values due to limitations of the physics-based drainage models for representing individual, point-scale measurements (Hill et al., 2025b). Given the sensitivity that we find between ice flow and five key GlaDS parameters (Table 1; Fig. 7), it is important to further consider the role of parametric uncertainty in ice-flow projections. The form of the Budd friction parameterization (Eq. 2) means that low effective pressure causes low basal drag only if the friction coefficient C is not relatively large to compensate. In the parameter sensitivity experiment shown in Fig. 7(c), the friction coefficient is adjusted for each parameter combination in order to match present-day conditions, leading to the opposite impact of parameter variations than suggested by standalone subglacial drainage modelling. The inverted sensitivity makes it challenging to relate subglacial hydrologic processes to ice-sheet changes. For instance, a model configuration that produces larger channels and higher effective pressure might result in faster flow under future conditions than a model with fewer small channels and lower effective pressure. This sensitivity is a consequence of the unknown friction coefficient that must be inferred. To first order, uncertainty in ice flow stemming from subglacial conditions could be assessed using the low-end (static N) and high-end (perfect ocean connection) members to estimate the total range of plausible outcomes, along with a simulation with conventional GlaDS parameters to estimate an intermediate outcome. Since the random forest makes fast predictions of effective pressure for various GlaDS parameter values, it is ideally suited for a more detailed uncertainty quantification study, for instance to quantify the uncertainty arising from unconstrained hydrology model parameters against that from other processes.

https://doi.org/10.5194/egusphere-2026-343
Preprint. Discussion started: 3 March 2026

4.3 Random forest model

When ice speeds are used as the evaluation metric, the random forest parameterization closely matches results obtained using GlaDS directly ($R^2 = 0.99$ in both present and future experiments, Table 3, 4). The random forest parameterization has lower fidelity in terms of effective pressure ($R^2 = 0.65$), but remains significantly better than simple assumptions such as the perfect ocean connection model ($R^2 = -74$) or assuming a constant flotation fraction ($R^2 \leq 0$; Table C2) while not being noticeably more expensive than using these simple assumptions.

The nearly exclusive sensitivity of the random forest to the ice thickness is unexpected in the context of classical glacier hydrology, but may be in part due to the choice of using flotation fraction and effective pressure, which both depend on ice thickness, as the variables describing the drainage system. It might have been expected, for instance, that the random forest would depend more strongly on the Shreve potential and its gradient (Shreve, 1972), given the role of hydraulic potential and its gradient in GlaDS as well as the GlaDS prediction of high subglacial water pressures over much of the domain. However, linking feature importance rankings to physical justifications is challenging with correlated and linearly dependent features. In fact, similar prediction performance can be obtained by removing ice thickness as a feature. In that case, several features, including the Shreve potential, but not its gradient, collectively influence predictions (Fig. D3). The surface slope, which is a major determinant of the potential slope, has nonzero importance, but is still only a minor contributor to predictions, with the bed elevation becoming the most important. The predictive power of ice thickness in terms of flotation fraction and effective pressure that we have found is not unprecedented. Based on GlaDS simulations for Denman Glacier, McArthur et al. (2023) fit a site-specific algebraic parameterization of flotation fraction that depends solely on ice thickness. The random forest parameterization presented here generalizes the functional form of this relationship and extends its applicability, while sharing the strong dependence on ice thickness.

Any number of models, most notably convolutional or graph neural networks, could have been used in place of the random forest. Considering the success that Verjans and Robel (2024) report for a convolutional neural network (CNN) emulator of GlaDS that is trained on several basins in Greenland, the random forest serves as a complementary, statistically simpler approach. Both approaches allow for spatial and temporal transferability to basins and ice-sheet states unseen during training. Verjans and Robel (2024) add transferability to different surface melt forcing timeseries, while we include parameter uncertainty in our investigation. Even with tens of millions of training values, the random forest is fast to train ($\sim$2 minutes on a single CPU), has a light memory footprint (< 1 GB), and is extremely fast for predictions (21 seconds on a single CPU continent-wide at finer resolution than state-of-the-art ice-sheet models). The fast training naturally allows for exploratory analysis, facilitating cross-validation and complete quantification of the sensitivity to the basins used for training (Fig. 4). Despite the simpler approach we take, which notably does not use neighbour information in training or making predictions, we find similar performance in terms of hydraulic potential ($R^2 = 0.99$ in this study compared to $R^2 = 0.96$ in Verjans and Robel (2024)) and ice-flow speeds ($R^2 = 0.99$ in this study compared to $R^2 = 0.96$).

Previous work has also shown higher fidelity for emulating GlaDS flotation fraction using Gaussian processes (Hill et al., 2025a, b) than achieved with the random forest parameterization. However, these Gaussian process emulators have been site-

https://doi.org/10.5194/egusphere-2026-343
Preprint. Discussion started: 3 March 2026

specific, with no ability to generalize beyond the precise catchment and ice-sheet geometry used for training. With the random forest parameterization, we are focusing on constructing a parameterization that is relevant for coupling with ice flow, which requires the ability to generalize in space and for unseen ice-sheet conditions as in the experiments with perturbed ice-sheet geometries. While some fidelity is lost in emulating subglacial hydrology variables, the performance in reproducing ice-flow speeds meets or exceeds that of higher fidelity hydrology emulators.

4.4 Limitations

4.4.1 Model configurations

The random forest parameterization inherits the limitations of the GlaDS model configuration. For instance, GlaDS is incapable of representing hydraulically disconnected behaviour, which has been shown to be a primary control on seasonality of some Greenland outlet glaciers (Murray and Clarke, 1995; Andrews et al., 2014; Hill et al., 2025b) and is likely important in Antarctica. Since GlaDS assumes drainage over a hard bed, we are overlooking the influence of heterogeneity in the bed type (e.g., Muto et al., 2019) on hydrology (e.g., Kazmierczak et al., 2024).

For the ice-flow experiments, we do not include full two-way coupling between hydrology and the ice-sheet model (e.g., Hoffman and Price, 2014), in either the case of the random forest parameterization or the GlaDS simulations. We have used a simplified ice-sheet model configuration consisting of the depth-integrated SSA approximation to the momentum balance, rather than a higher-order depth-resolved model, combined with a nonlinear Budd friction parameterization, as opposed to a more physically justified regularized Coulomb parameterization.

For the 2050 and 2300 GlaDS simulations, present-day basal melt rates and slip speeds are used to run the hydrology model. The resultant effective pressure is used in the friction parameterization to compute future flow speeds, which introduce some inconsistency. The random forest parameterization implicitly includes these same assumptions since it is trained on present-day GlaDS simulations.

The basal melt rate that we use implicitly assumes that the bed is temperate and that all geothermal and frictional heat is used for melting. Minimum melt rates are therefore on the order of $\sim 4\,\mathrm{mm\,a^{-1}}$, even where the bed is likely frozen. Moreover, by running GlaDS for entire ice-flow basins and making random forest predictions for the entire continent, we are explicitly assuming that the bed is thawed according to the model's assumptions. Recent estimates of the Antarctic basal thermal state differ widely (Dawson et al., 2022; Raspoet and Pattyn, 2025; Seiner et al., 2025), with the best estimate that West Antarctica is predominantly warm-based and large swaths of East Antarctica are likely cold-based. To avoid over-analyzing results where the warm-bed assumption breaks down, we have assessed hydrology and ice flow near the grounding lines of major ice streams that are almost certainly warm-based. For interior regions that experience little change in thickness or speed, the inferred friction coefficient may partially compensate for errors in the warm-bed approximation. However, errors may be larger where the basal thermal state changes as the ice sheet evolves.

By limiting our scope to speeds over grounded ice and training the random forest parameterization to predict effective pressure, we are excluding the impact of subglacial grounding-line discharge on ice-shelf basal melting and stability. For

https://doi.org/10.5194/egusphere-2026-343
Preprint. Discussion started: 3 March 2026

instance, Pelle et al. (2024) conclude that the influence of subglacial drainage on ice-shelf melt exerts a greater control on ice-sheet evolution and mass loss than changes in effective pressure beneath grounded ice. To include these effects in ice-sheet model projections, the effective-pressure parameterization developed here could be extended to predict channelized and distributed grounding-line discharge along with effective pressure. Alternatively, the predictions could be converted back into hydraulic potential to drive water-routing algorithms as an intermediate step to derive discharge fields.

4.4.2 Perturbed geometry experiments

The thickness change, taken as the central estimate of Hillebrand et al. (2025b), relates to a different initial condition than the BedMachine v3 initial condition. Hillebrand et al. (2025b) use BedMap2 (Fretwell et al., 2013) for their initial state in the Amundsen Sea sector, while using BedMachine v3 for their initial state elsewhere, to obtain an initial condition nominally representative of 2000 and to correct stronger-than-observed retreat in the Amundsen Sea in their historical runs. This initial condition is relaxed for 10 years before beginning the projection runs. Rather than using their relaxed initial condition for present-day conditions, we take the more conventional route for hydrology modelling and use the BedMachine v3 state directly. Other processes that modify the ice-sheet geometry, such as gravitational, rotation and deformational effects (e.g., Han et al., 2025), have not been tested here but should be able to be implicitly accounted for through their impact on the random forest features.

There is some inconsistency in prescribing the same perturbed geometry for all effective-pressure treatments. Based on the different speeds, each effective-pressure treatment would result in different ice thickness at 2050 and 2300 in transient simulations. The limitations of incomplete coupling and inconsistent geometry should be addressed in future work that carries out transient, fully coupled simulations with the random forest hydrology parameterization.

As the atmosphere warms, it is likely that surface melt will occur over grounded ice at lower elevations (e.g., Dunmire et al., 2022). Should surface melt gain access to the bed, this would be another major difference for simulations that include active subglacial hydrology. It could be possible for future studies to add this effect to the random forest parameterization by adding a feature such as total annual surface melt, and by designing the ensemble of training simulations to include scenarios with and without surface melt accessing the bed. In this case, it is unlikely that using solely present-day simulations to train the parameterization would accurately capture future behaviour in response to surface melt inputs.

4.5 Perspectives on subglacial hydrology parameterizations

The agreement between ice speeds obtained using GlaDS and the random forest parameterization of subglacial hydrology is encouraging for the expanded application of such parameterizations. Adopting machine-learning parameterizations of subglacial hydrology that are significantly more accurate, but not substantially more expensive, than the perfect ocean connection or constant flotation fraction parameterizations will lead to more realistic basal drag-related ice-sheet changes. Since the subglacial drainage model ensemble used for training is run offline and in parallel, the computational cost is manageable and is incurred only once. The trained parameterization makes the cost of adding active subglacial hydrology to an ice-sheet model almost negligible; continent-wide predictions at typical ice-sheet model resolutions (≥ 4 km) take only a few seconds.

https://doi.org/10.5194/egusphere-2026-343
Preprint. Discussion started: 3 March 2026

Perhaps just as important as the computational savings are the vastly simplified logistics of using a parameterization rather than the numerical model. Running a subglacial hydrology model, the user inevitably confronts a unique and distinct set of challenges and setbacks from what they might experience running the ice-flow model alone. Using the pre-trained random forest parameterization is simple in comparison, since issues related to numerical convergence, boundary conditions and forcing have already been addressed in generating the training data. However, tightly coupling the random forest parameterization to ice flow introduces software challenges. The random forest parameterization, constructed using scikit-learn (Pedregosa et al., 2011), is not directly operable with the ISSM source code. This is a surmountable problem, but is beyond the scope of this work.

Should the random forest be integrated within the ice-sheet model source code, care should be taken when it is used in place of GlaDS. Since it has not been tested as part of transient projections, coupled projections using GlaDS should be used for evaluation, whether at basin-scale or continental. The deviation from present-day ice-sheet thickness should be monitored to avoid extrapolation outside the feature space encountered during training. For the purpose of long-term projections, the GlaDS ensembles that were presented here for evaluation at 2050 (WAIS) and 2300 (EAIS) could be used for additional training data to further avoid extrapolation.

5 Conclusions

We have presented and evaluated a statistical parameterization that emulates the GlaDS physics-based subglacial drainage model for the Antarctic Ice Sheet. The parameterization predicts effective pressure for arbitrary ice-sheet geometries and as a function of model parameter values. The statistical model, a random forest regressor, is trained using 100 GlaDS simulations in seven major ice-flow basins and can be used to predict continent-wide effective pressure. We evaluate the effective pressure predictions for present-day and plausible future ice-sheet states against those predicted by GlaDS, and use the effective pressure as input to an ice-sheet model to assess the similarity of modelled ice speeds.

Across the seven ice-flow basins and five uncertain GlaDS parameters, the random forest parameterization captures 80% of the GlaDS-simulated flotation fraction variations and 65% of the effective pressure variations. Based on feature importance metrics, the random forest parameterization primarily learns a mapping between ice thickness and flotation fraction, with other geometric factors exerting a secondary control. In present-day ice-sheet model experiments with an effective pressure-dependent basal friction parameterization, substituting the random forest parameterization in place of the GlaDS model captures 99% of the variance in modelled ice speed. Applying thickness change drawn from ice-sheet model projections to 2050 (West Antarctica) and 2300 (East Antarctica) shows that the random forest has similar performance for future ice-sheet states as it does under present-day conditions, and that it closely reproduces the speeds obtained using the physics-based model with grounding-line speed errors of 2.1–10%.

The random forest parameterization is a tool that allows for coupled hydrology–dynamics projections at spatial and temporal scales that would be burdensome to infeasible using the physics-based hydrology model directly. Its interface is simpler than running numerical simulations, as it depends only on geometric quantities easily extracted from ice-sheet model inputs. Given the success that we have illustrated for reproducing grounding-line speed, an important extension would be to make projec-

https://doi.org/10.5194/egusphere-2026-343
Preprint. Discussion started: 3 March 2026

tions of ice-sheet evolution, using the random forest to predict effective-pressure changes, with the eventual goal of routinely including dynamic subglacial drainage in ice-sheet model projections.

https://doi.org/10.5194/egusphere-2026-343
Preprint. Discussion started: 3 March 2026

Appendix A: Evaluation of channelized grounding-line discharge

Table A1 and Fig. A1 evaluate the grounding-line channel discharge from the perturbed-parameter ensemble against published values from the literature. While the ensemble encompasses previously reported values, the major west Antarctic basins are biased to lower channel discharge than reported elsewhere. Parameter values that are varied in the ensemble are listed in Table 1 and fixed parameters are listed in Table A2

Table A1. Reference grounding line discharge from subglacial drainage modelling studies. The coordinates indicate the location of maximum channel discharge in the simulations presented here and are presented in Antarctic Polar Stereographic projection.

Glacier	Coordinates (km E, km N)	Mean Q ($m^3\,s^{-1}$)	Sources ($m^3\,s^{-1}$)	
Thwaites	-1519.7, -463.4	92	127 ± 24	(Hager et al., 2022)
			80	(Dow, 2022)
			69	(Ehrenfeucht et al., 2025)
Pine Island	-1583.8, -258.3	42.5	40	(Dow, 2022)
			45	(Ehrenfeucht et al., 2025)
Denman	2520.3, -411.2	14.1	9.5	(Pelle et al., 2023)
			15.8	(McArthur et al., 2023)
			17	(Ehrenfeucht et al., 2025)
Totten	2267.5, -994.0	30.3	35.82	(Pelle et al., 2024)
			24.7	(Dow et al., 2020)
Lambert	1677.3, 708.2	202	202	(Ehrenfeucht et al., 2025)
Rutford	-1263.5, 155.3	47	47	(Ehrenfeucht et al., 2025)
Academy	-956.6, 252.9	45.1	24.2	(Dow et al., 2022)
			66	(Ehrenfeucht et al., 2025)
Recovery	-573.5, 776.4	82	82	(Ehrenfeucht et al., 2025)

Appendix B: Friction inversions

Basal friction inversions use a cost function consisting of squared speed error and log-speed error combined with Tikhonov regularization,

$$\mathcal{J} = \mathcal{J}_{\mathrm{u}} + \gamma \mathcal{J}_{\log u} + \alpha \mathcal{J}_{\mathrm{reg}} \tag{B1}$$

$$= \int_{\Omega} \frac{1}{2} |\mathbf{u} - \mathbf{u}_{\mathrm{obs}}|^2 \, dA + \gamma \int_{\Omega} \left(\log \frac{|\mathbf{u}| + \varepsilon}{|\mathbf{u}_{\mathrm{obs}}| + \varepsilon} \right)^2 dA + \alpha \int_{\Omega} \frac{1}{2} |\nabla C|^2 dA, \tag{B2}$$

for domain Ω, modelled velocity $\mathbf{u}$, observed velocity $\mathbf{u}_{\mathrm{obs}}$, spatially varying friction coefficient C, and with $\varepsilon = 2 \times 10^{-16}$. The logarithmic misfit weight $\gamma = 10^{-3}$ (except $\gamma = 10^{-2}$ in the Amundsen Sea sector, basin G-H) is chosen to achieve a

https://doi.org/10.5194/egusphere-2026-343
Preprint. Discussion started: 3 March 2026

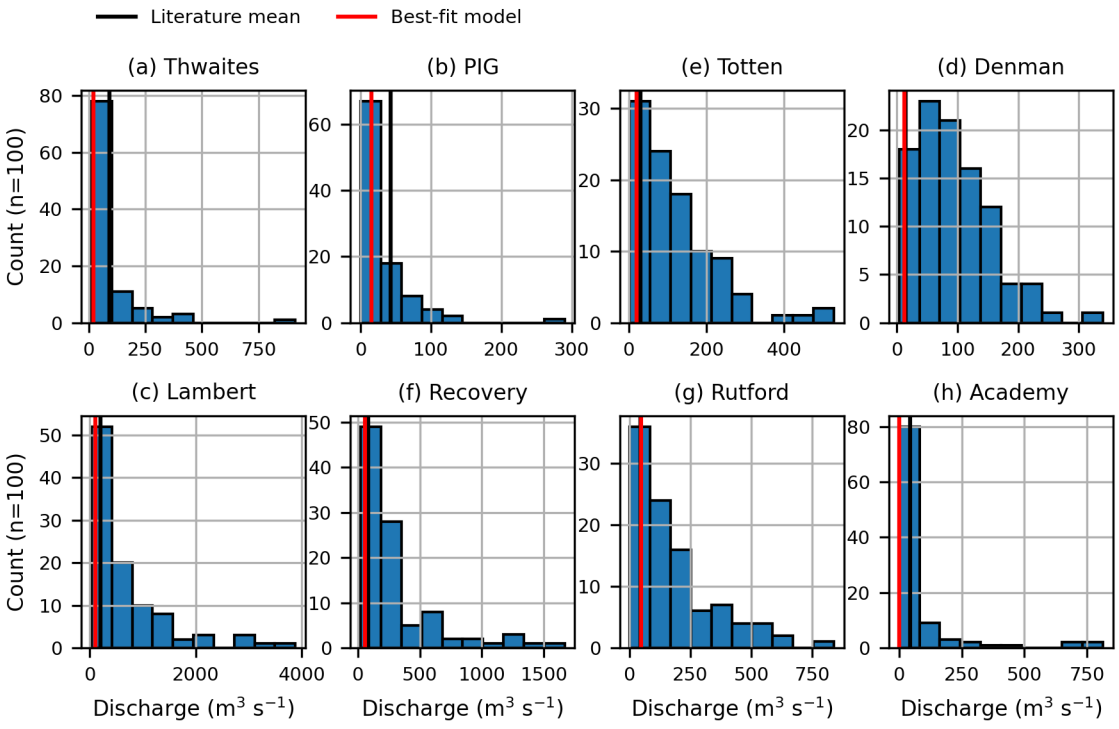

Figure A1. Modelled channelized discharge crossing the grounding line for select outlet glaciers compared to published modelling studies. See Table A1 for the sources of the literature values.

similar order-of-magnitude contribution from both the squared error and logarithmic cost functions. The regularization weight α is chosen from L-curve analysis (e.g., Wolovick et al., 2023) (Fig. B1).

https://doi.org/10.5194/egusphere-2026-343
Preprint. Discussion started: 3 March 2026

Table A2. Physical constants (top group) and fixed model parameters (bottom group)

	Parameter	Value	Units
ρ_w	Density of freshwater	1000	$kg\,m^{-3}$
ρ_{sw}	Density of seawater	1023	$kg\,m^{-3}$
ρ_i	Density of ice	917	$kg\,m^{-3}$
g	Gravitational acceleration	9.81	$m\,s^{-2}$
L	Latent heat of fusion	3.34×10^5	$J\,kg^{-1}$
c_w	Specific heat capacity of water	4.22×10^3	$J\,kg^{-1}$
c_t	Pressure melting coefficient	-7.50×10^{-8}	$K\,Pa^{-1}$
ν	Kinematic viscosity of water at 0°C	1.793×10^{-6}	$m^2\,s^{-1}$
α_c	Channel-flow exponent	$\frac{5}{4}$	–
β_c	Channel-flow exponent	$\frac{3}{2}$	–
h_s	Bed bump height	0.25	m
n	Ice-flow exponent	3	–
ω	Laminar–turbulent transition parameter	5.0×10^{-4}	–
e_v	Englacial void fraction	1.0×10^{-5}	–
A	Flow-law coefficient for ice at the pressure-melting temperature	2.4×10^{-24}	$Pa^{-3}\,s^{-1}$
p	Basal slip-speed exponent	5	–

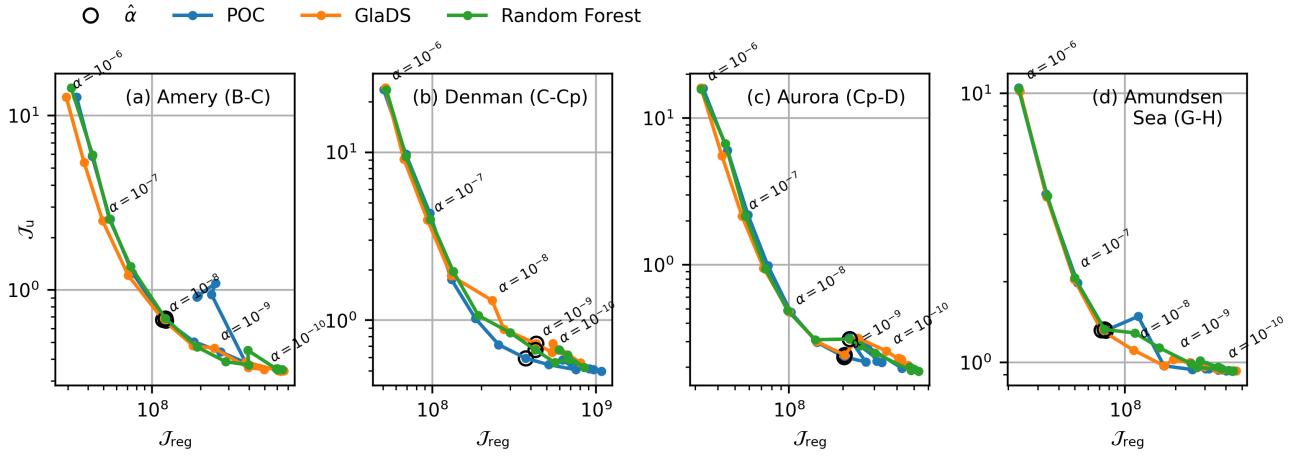

Figure B1. L-curve analysis. Regularization ($\mathcal{J}_{reg}$) and absolute misfit ($\mathcal{J}_u$) cost functions for friction inversions with perfect ocean connection (POC) effective pressure, effective pressure modelled with GlaDS, and effective pressure predicted with the random forest. The chosen values $\hat{\alpha}$ are marked with black circles.

https://doi.org/10.5194/egusphere-2026-343
Preprint. Discussion started: 3 March 2026

Table C1. Cross-validation evaluation of the random forest model trained on the mean of the perturbed-parameter ensemble. Coefficient of variation R^2 values are computed using GlaDS simulated values as the reference.

	f_w			N		
Basin	All	$u > 200\,\mathrm{m\,a^{-1}}$	Gridded	All	$u > 200\,\mathrm{m\,a^{-1}}$	Gridded
Amundsen Sea (G-H)	0.91	0.83	0.91	0.58	0.74	0.45
Amery (B-C)	0.92	0.90	0.95	0.66	0.54	0.77
Denman (C-Cp)	0.90	0.96	0.92	0.59	0.86	0.62
Aurora (Cp-D)	0.92	0.95	0.90	0.71	0.94	0.71
Recovery (Jpp-K)	0.90	0.91	0.93	0.53	0.71	0.56
Siple (Ep-F)	0.89	0.86	0.88	0.70	0.91	0.26
Filchner-Ronne (J-Jpp)	0.90	0.91	0.90	0.68	0.81	0.45
Overall	0.90	0.91	0.91	0.63	0.80	0.56

Table C2. Coefficient of variation (R^2) for the random forest parameterization, the perfect ocean connection model, and constant flotation fraction fields.

N parameterization	R^2
Ensemble-mean random forest	0.63
Perfect ocean connection	-74
85% flotation fraction	-2.96
95% flotation fraction	-0.48

Appendix C: Random forest parameterization trained on the ensemble mean

This section evaluates the random forest parameterization that is trained to predict the ensemble-average effective pressure. This is the random forest used to compute the quantities in Fig. 3 and 4. Compared to the complete random forest parameterization evaluated in Table 3, the ensemble-mean random forest has higher R^2 values for flotation fraction (0.90 here compared to 0.85 including subglacial hydrology model parameters), slightly lower R^2 for domain-wide effective pressure (0.63 compared to 0.65), and higher R^2 values where surface speeds exceed $200\,\mathrm{m\,a^{-1}}$ (Table C1).

Table C2 compares the ensemble-mean random forest to the perfect ocean connection model and assuming a constant flotation fraction. The random forest is the only model that achieves better performance than using the spatially uniform mean ($R^2 = 0$).

The ensemble-average random forest (Fig. C1) is more accurate than the full random forest (Fig. 7) at emulating speeds obtained using GlaDS directly. Table C3 compares the grounding-line speed error, highlighting the reduced absolute and

https://doi.org/10.5194/egusphere-2026-343
Preprint. Discussion started: 3 March 2026

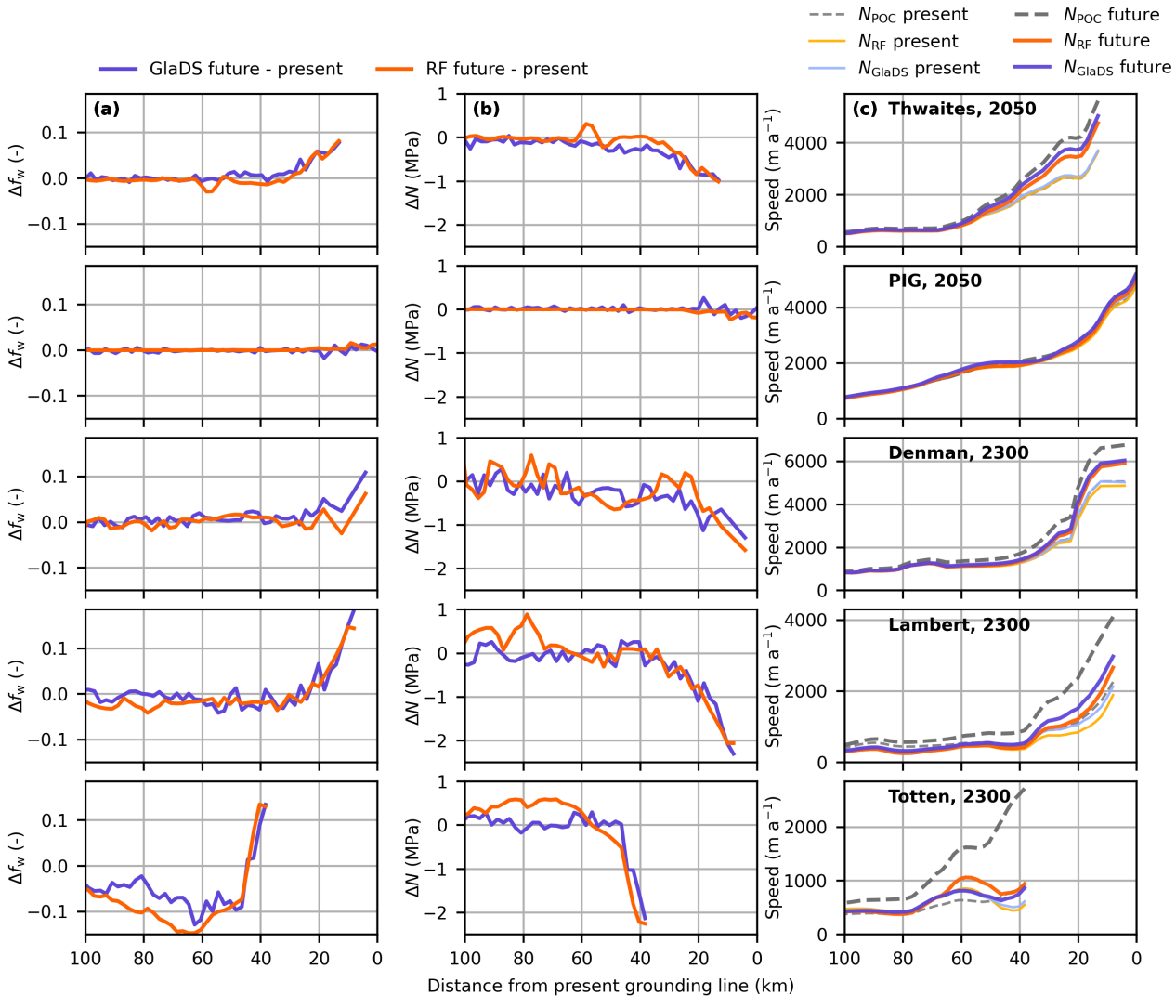

Figure C1. Sensitivity of ice speed to effective pressure for representative future ice-sheet geometries and for the ensemble-mean random forest parameterization. (column a) Flotation fraction difference from present day and (column b) effective pressure difference from present day simulated by GlaDS and predicted by the random forest (RF). (column c) Modelled speed corresponding to static and evolving GlaDS, random forest (RF) and perfect ocean connection (POC) effective pressure fields. Refer to Fig. 1(d) for flowline locations.

relative errors. Aside from Totten Glacier, where the friction coefficient is unconstrained, the mean-only random forest has grounding-line speed error below 7%, while the full random forest has error below 10%.

https://doi.org/10.5194/egusphere-2026-343
Preprint. Discussion started: 3 March 2026

Table C3. Absolute and relative grounding-line speed error when using the random forest (RF) trained on the ensemble-mean and the full random forest that includes five uncertain GlaDS parameters

	Full RF		Mean-only RF	
Profile	Absolute error ($m\,a^{-1}$)	Relative error (%)	Absolute error ($m\,a^{-1}$)	Relative error (%)
Thwaites	272	5.4	78	1.6
Pine Island	148	2.8	28	0.55
Denman	127	2.1	137	2.3
Lambert	311	10	199	6.7
Totten	78	9.0	269	30

Appendix D: Random forest sensitivity analysis

Figure 3 used permutation feature importance, which summarizes the global impact of each feature, to identify the most important features and construct a simplified model. To more deeply investigate the relationships learned by the Random forest, we manually inspect individual decision trees (Fig. D1). This particular tree first partitions samples by surface slope. For ∼80% of samples with moderate surface slopes (left branch), the samples are further split by ice thickness and Shreve potential. For samples with high surface slope, samples are split by bed elevation and ice thickness (right branch). This branch, for instance, isolates areas with high bed elevations and low ice thickness and assigns low flotation fraction values (0.52). Since the random forest consists of trees that are trained using different subsets of the data and that consider random subsets of variables for each split, different trees should generally have different structures. Given the correlated and dependent features in the training data, the trees in our random forest have broadly similar structures.

To complement the global permutation feature importance values, we compute local Shapely Additive exPlanation (SHAP) values (Lundberg and Lee, 2017) for the ensemble-mean random forest flotation fraction predictions. SHAP values estimate the contribution of each feature to each prediction, resulting in maps of feature contributions (Fig. D2). Negative values indicate that increasing the feature value decreases the predicted flotation fraction relative to the mean, and positive values indicate that increasing the feature value increases the predicted flotation fraction. Features with larger absolute SHAP values more strongly contribute to the prediction. Using the Amundsen Sea basin as an example, the SHAP values reinforce that random forest is most sensitive to the ice thickness, especially in regions with simple ice-sheet geometry and in fast-flowing areas of Thwaites and Pine Island. Consistent with the decision tree structure, steep surface slopes and high bed elevations, as seen near the grounding line away from the Thwaites and Pine Island trunks and over subglacial volcanoes west of the main Thwaites trunk, are strong indicators of low flotation fraction.

Global (Fig. 3) and local (Fig. D2) feature importance metrics, and manual inspection of decision trees (Fig. D1) highlight ice thickness as the feature that the random forest most strongly relies on for predictions. However, since the ice thickness can be reconstructed as the difference between the surface and bed elevation features, we retrain the random forest without ice thickness to investigate the resulting global feature importance scores. The model with no ice thickness shows stronger

https://doi.org/10.5194/egusphere-2026-343
Preprint. Discussion started: 3 March 2026

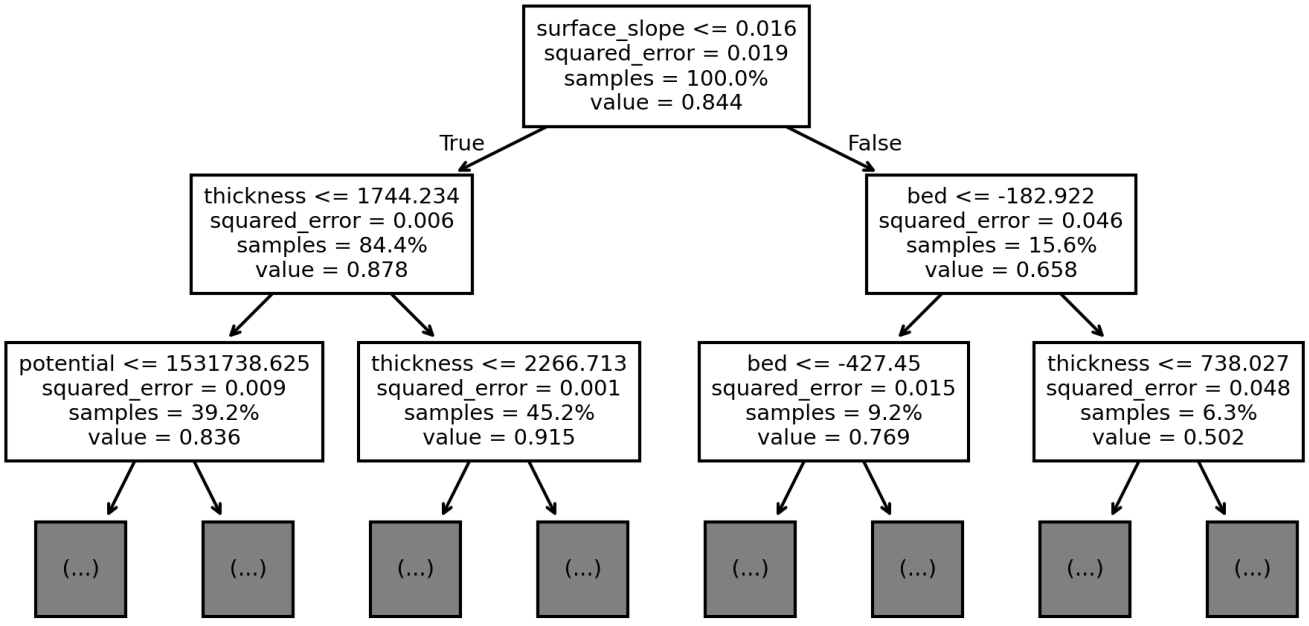

Figure D1. Top three levels of a representative decision tree from the ensemble-mean random forest model. By splitting on one variable at a time, up to 10 layers deep, the random forest partitions the feature space into rectangles. Within each partition, the prediction is the mean of all training samples. Each split is labelled with the feature name (e.g., surface slope for the top-level node), the squared error from out-of-bag samples, the proportion of samples that reach the split, and the mean value of samples that reach the split. Ellipses indicate that the tree continues below the levels shown.

sensitivity to the bed elevation, surface elevation, grounding-line distance, and surface slope (Fig. D3) than the model with ice thickness (Fig. 3), and lower sensitivity to the Shreve potential. The increased sensitivity to bed and surface elevations suggests that the random forest learns to reconstruct ice thickness based on other features, highlighting that the relationship between flotation fraction, effective pressure, and ice thickness is robust. Further interpretation remains challenging among the remaining interdependent features. For instance, the Shreve potential is a linear combination of the surface and bed elevations, so we cannot rule out dependence on the Shreve potential through its constituent terms.

https://doi.org/10.5194/egusphere-2026-343
Preprint. Discussion started: 3 March 2026

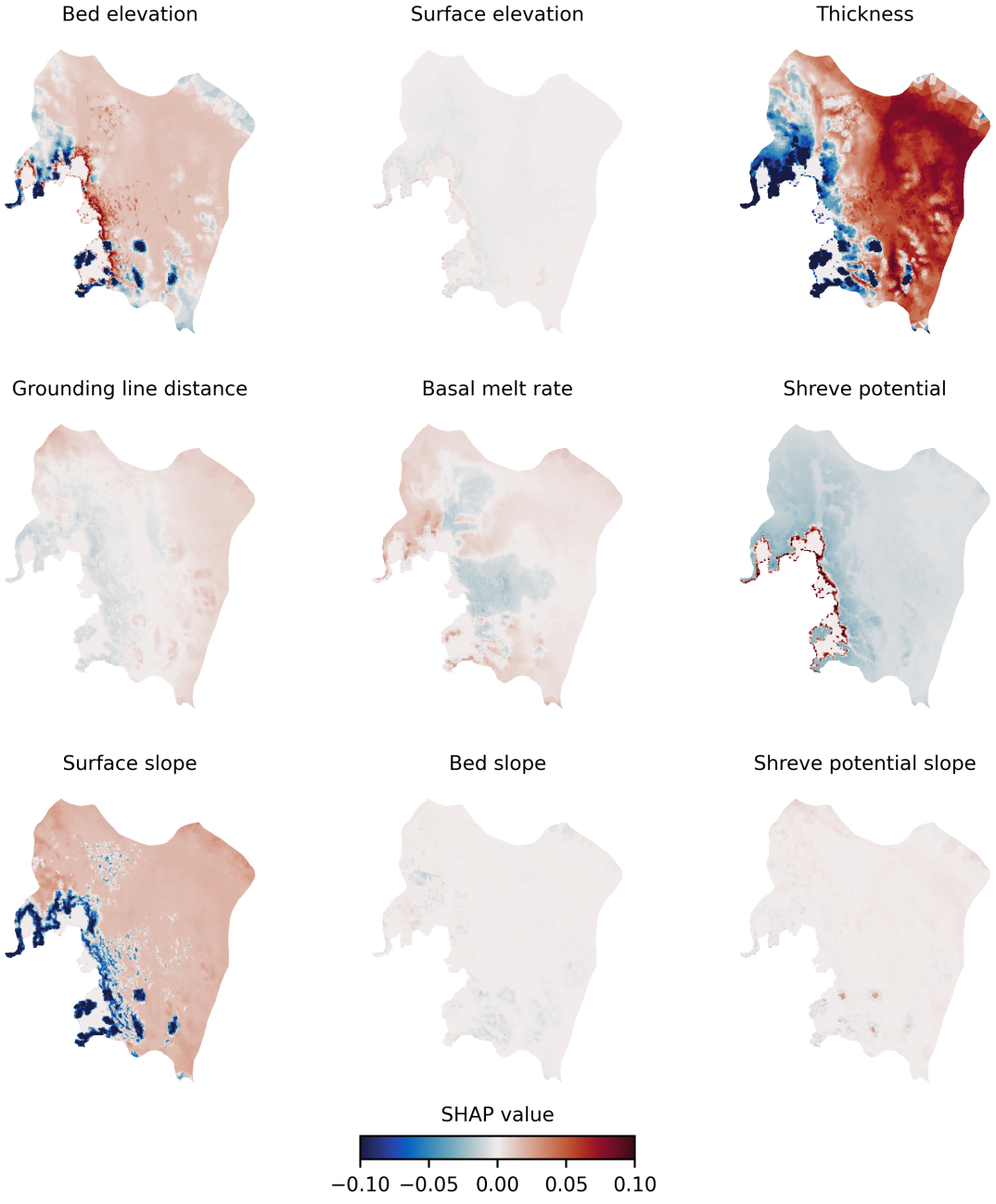

Figure D2. Shapley Additive exPlanation (SHAP) values (Lundberg and Lee, 2017) for the Amundsen Sea basin. Strongly positive or negative values indicate locally important features and the sign corresponds to the direction of influence on the prediction.

https://doi.org/10.5194/egusphere-2026-343
Preprint. Discussion started: 3 March 2026

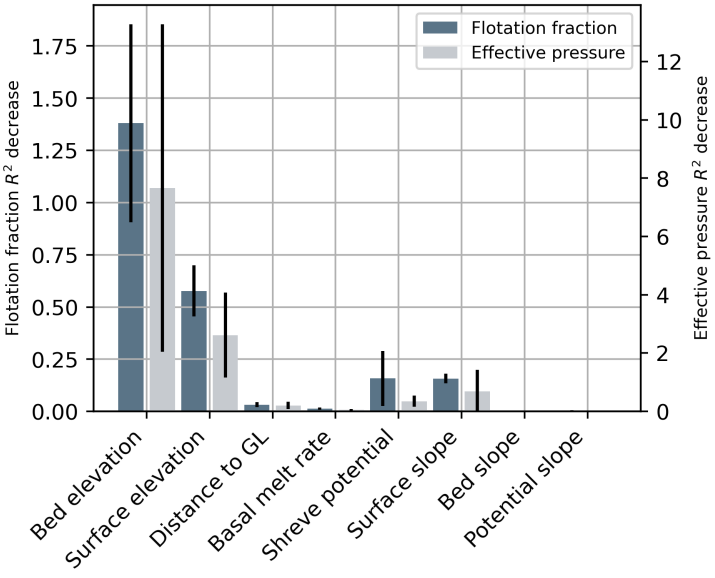

Figure D3. Feature importance for the ensemble-mean random forest parameterization when excluding ice thickness as a feature.

https://doi.org/10.5194/egusphere-2026-343
Preprint. Discussion started: 3 March 2026

Code and data availability. BedMachine Antarctica v3 data are available at https://doi.org/10.5067/FPSU0V1MWUB6 (Morlighem, 2022). Ice flow velocities from Rignot et al. (2011b) used for friction coefficient inversions are available at https://doi.org/10.5067/D7GK8F5J8M8R (Rignot et al., 2017). The ISSM v4.24 model is available at https://github.com/ISSMteam/ISSM (Larour et al., 2012). Ice-sheet projections to 2300 for experiment "expAE03_04_q05m50" from Hillebrand et al. (2025b) are available at https://doi.org/10.5281/zenodo.16798097 (Hillebrand et al., 2025a).

All code and model data produced in this study, including scripts to generate figures, are available at https://doi.org/10.5281/zenodo.18381581 (Hill et al., 2026).

Author contributions. GF and DB conceived of the idea of emulating subglacial drainage models with input from TH. TH designed the experiments in consultation with MH, GF and DB. TH configured the GlaDS ensembles with input from MH and GF. TH ran the simulation ensembles, fit random forest models, computed ice-flow solutions and analyzed the outputs. MH verified ice-flow solutions and contributed to their interpretation with TH and GF. All authors reviewed final interpretations and analysis. TH prepared the manuscript. All authors edited and revised the manuscript.

Competing interests. The authors declare that they have no conflict of interest.

Acknowledgements. TH was supported by Simon Fraser University and the Natural Sciences and Engineering Research Council of Canada (NSERC) Canada Graduate Scholarship program. GF and DB received support from the NSERC Discovery Grants program. Support for MH was provided through the Scientific Discovery through Advanced Computing (SciDAC) program funded by the U.S. Department of Energy (DOE), Office of Science, Advanced Scientific Computing Research and Biological and Environmental Research Programs. This research was enabled in part by support provided by WestDRI (https://training.westdri.ca), Calcul Quebec (https://www.calculquebec.ca/) and the Digital Research Alliance of Canada (https://alliancecan.ca).

https://doi.org/10.5194/egusphere-2026-343
Preprint. Discussion started: 3 March 2026

References

Andrews, L. C., Catania, G. A., Hoffman, M. J., Gulley, J. D., Lüthi, M. P., Ryser, C., Hawley, R. L., and Neumann, T. A.: Direct observations of evolving subglacial drainage beneath the Greenland Ice Sheet, Nature, 514, 80–83, https://doi.org/10.1038/nature13796, 2014.

Asay-Davis, X. S., Cornford, S. L., Durand, G., Galton-Fenzi, B. K., Gladstone, R. M., Gudmundsson, G. H., Hattermann, T., Holland, D. M., Holland, D., Holland, P. R., Martin, D. F., Mathiot, P., Pattyn, F., and Seroussi, H.: Experimental design for three interrelated marine ice sheet and ocean model intercomparison projects: MISMIP v. 3 (MISMIP+), ISOMIP v. 2 (ISOMIP+) and MISOMIP v. 1 (MISOMIP1), Geoscientific Model Development, 9, 2471–2497, https://doi.org/10.5194/gmd-9-2471-2016, 2016.

Breiman, L.: Random forests, Machine Learning, 45, 5–32, https://doi.org/10.1023/A:1010933404324, 2001.

Brondex, J., Fillet-Chaulet, F., and Gagliardini, O.: Sensitivity of centennial mass loss projections of the Amundsen basin to the friction law, The Cryosphere, 13, 177–195, https://doi.org/10.5194/tc-13-177-2019, 2019.

Budd, W. F., Keage, P. L., and Blundy, N. A.: Empirical studies of ice sliding, Journal of Glaciology, 23, 157–170, https://doi.org/10.3189/S0022143000029804, 1979.

Dawson, E. J., Schroeder, D. M., Chu, W., Mantelli, E., and Seroussi, H.: Ice mass loss sensitivity to the Antarctic ice sheet basal thermal state, Nature Communications, 13, 4957, https://doi.org/10.1038/s41467-022-32632-2, 2022.

de Fleurian, B., Gagliardini, O., Zwinger, T., Durand, G., Le Meur, E., Mair, D., and Råback, P.: A double continuum hydrological model for glacier applications, The Cryosphere, 8, 137–153, https://doi.org/10.5194/tc-8-137-2014, 2014.

Dow, C., McCormack, F., Young, D., Greenbaum, J., Roberts, J., and Blankenship, D.: Totten Glacier subglacial hydrology determined from geophysics and modeling, Earth and Planetary Science Letters, 531, 115 961, https://doi.org/10.1016/j.epsl.2019.115961, 2020.

Dow, C. F.: The role of subglacial hydrology in Antarctic ice sheet dynamics and stability: a modelling perspective, Annals of Glaciology, 63, 49–54, https://doi.org/10.1017/aog.2023.9, 2022.

Dow, C. F., Ross, N., Jeofry, H., Siu, K., and Siegert, M. J.: Antarctic basal environment shaped by high-pressure flow through a subglacial river system, Nature Geoscience, 15, 892–898, https://doi.org/10.1038/s41561-022-01059-1, 2022.

Downs, J. and Johnson, J. V.: A rapidly retreating, marine-terminating glacier's modeled response to perturbations in basal traction, Journal of Glaciology, 68, 891–900, https://doi.org/10.1017/jog.2022.5, 2022.

Dunmire, D., Lenaerts, J. T. M., Datta, R. T., and Gorte, T.: Antarctic surface climate and surface mass balance in the Community Earth System Model version 2 during the satellite era and into the future (1979–2100), The Cryosphere, 16, 4163–4184, https://doi.org/10.5194/tc-16-4163-2022, 2022.

Ehrenfeucht, S., Dow, C., McArthur, K., Morlighem, M., and McCormack, F. S.: Antarctic Wide Subglacial Hydrology Modeling, Geophysical Research Letters, 52, e2024GL111 386, https://doi.org/10.1029/2024GL111386, 2025.

Fischler, Y., Kleiner, T., Bischof, C., Schmiedel, J., Sayag, R., Emunds, R., Oestreich, L. F., and Humbert, A.: A parallel implementation of the confined–unconfined aquifer system model for subglacial hydrology: design, verification, and performance analysis (CUAS-MPI v0.1.0), Geoscientific Model Development, 16, 5305–5322, https://doi.org/10.5194/gmd-16-5305-2023, 2023.

Fretwell, P., Pritchard, H. D., Vaughan, D. G., Bamber, J. L., Barrand, N. E., Bell, R., Bianchi, C., Bingham, R. G., Blankenship, D. D., Casassa, G., Catania, G., Callens, D., Conway, H., Cook, A. J., Corr, H. F. J., Damaske, D., Damm, V., Ferraccioli, F., Forsberg, R., Fujita, S., Gim, Y., Gogineni, P., Griggs, J. A., Hindmarsh, R. C. A., Holmlund, P., Holt, J. W., Jacobel, R. W., Jenkins, A., Jokat, W., Jordan, T., King, E. C., Kohler, J., Krabill, W., Riger-Kusk, M., Langley, K. A., Leitchenkov, G., Leuschen, C., Luyendyk, B. P., Matsuoka, K., Mouginot, J., Nitsche, F. O., Nogi, Y., Nost, O. A., Popov, S. V., Rignot, E., Rippin, D. M., Rivera, A., Roberts, J., Ross, N., Siegert, M. J.,

https://doi.org/10.5194/egusphere-2026-343
Preprint. Discussion started: 3 March 2026

Smith, A. M., Steinhage, D., Studinger, M., Sun, B., Tinto, B. K., Welch, B. C., Wilson, D., Young, D. A., Xiangbin, C., and Zirizzotti, A.: Bedmap2: improved ice bed, surface and thickness datasets for Antarctica, The Cryosphere, 7, 375–393, https://doi.org/10.5194/tc-7-375-2013, 2013.

Gagliardini, O., Cohen, D., Råback, P., and Zwinger, T.: Finite-element modeling of subglacial cavities and related friction law, Journal of Geophysical Research: Earth Surface, 112, F02 027, https://doi.org/10.1029/2006JF000576, 2007.

Hager, A. O., Hoffman, M. J., Price, S. F., and Schroeder, D. M.: Persistent, extensive channelized drainage modeled beneath Thwaites Glacier, West Antarctica, The Cryosphere, 16, 3575–3599, https://doi.org/10.5194/tc-16-3575-2022, 2022.

Han, H. K., Hoffman, M., Asay-Davis, X., Hillebrand, T. R., and Perego, M.: Improving Projections of Antarctic Ice Sheet Contribution to Sea-Level Change Through 2300 by Capturing Gravitational, Rotational, and Deformational Effects, Journal of Geophysical Research: Earth Surface, 130, e2025JF008 388, https://doi.org/10.1029/2025JF008388, 2025.

Hewitt, I. J., Schoof, C., and Werder, M. A.: Flotation and free surface flow in a model for subglacial drainage. Part 2. Channel flow, Journal of Fluid Mechanics, 702, 157–187, https://doi.org/10.1017/jfm.2012.166, 2012.

Hill, T., Flowers, G. E., Hoffman, M. J., Bingham, D., and Werder, M. A.: Improved representation of laminar and turbulent sheet flow in subglacial drainage models, Journal of Glaciology, 70, e24, https://doi.org/10.1017/jog.2023.103, 2024.

Hill, T., Bingham, D., Flowers, G. E., and Hoffman, M. J.: Computationally efficient subglacial drainage modelling using Gaussian process emulators: GlaDS-GP v1.0, Geoscientific Model Development, 18, 4045–4074, https://doi.org/10.5194/gmd-18-4045-2025, 2025a.

Hill, T., Flowers, G. E., Bingham, D., and Hoffman, M. J.: Emulator-based Bayesian calibration of a subglacial drainage model, Annals of Glaciology, 66, e22, https://doi.org/10.1017/aog.2025.10016, 2025b.

Hill, T., Hoffman, M. J., Flowers, G. E., and Bingham, D.: timghill/antarctic-glads [code], Zenodo, https://doi.org/10.5281/zenodo.18381581, 2026.

Hillebrand, T., Hoffman, M., Han, H. K., Perego, M., Hager, A., Nolan, A., Asay-Davis, X., Price, S., Jerry, W., and Carlson, M.: MPAS-Albany Land Ice simulations of the Antarctic Ice Sheet through 2300: Exp02-05 state fields [Dataset], Zenodo, https://doi.org/10.5281/zenodo.16798097, 2025a.

Hillebrand, T. R., Hoffman, M. J., Han, H. K., Perego, M., Hager, A. O., Nolan, A., Asay-Davis, X., Price, S. F., Watkins, J., and Carlson, M.: Evolution of the Antarctic Ice Sheet from 2000–2300 and beyond: model sensitivity and uncertainty analysis using MPAS-Albany Land Ice, EGUsphere, 2025, 1–51, https://doi.org/10.5194/egusphere-2025-3942, 2025b.

Hoffman, M. J. and Price, S.: Feedbacks between coupled subglacial hydrology and glacier dynamics, Journal of Geophysical Research: Earth Surface, 119, 414–436, https://doi.org/10.1002/2013JF002943, 2014.

Hoffman, M. J., Perego, M., Price, S. F., Lipscomb, W. H., Zhang, T., Jacobsen, D., Tezaur, I., Salinger, A. G., Tuminaro, R., and Bertagna, L.: MPAS-Albany Land Ice (MALI): a variable-resolution ice sheet model for Earth system modeling using Voronoi grids, Geoscientific Model Development, 11, 3747–3780, https://doi.org/10.5194/gmd-11-3747-2018, 2018.

Iken, A.: The effect of the subglacial water pressure on the sliding velocity of a glacier in an idealized numerical model, Journal of Glaciology, 27, 407–421, https://doi.org/10.3189/S0022143000011448, 1981.

Joughin, I., Smith, B. E., and Holland, D. M.: Sensitivity of 21st century sea level to ocean-induced thinning of Pine Island Glacier, Antarctica, Geophysical Research Letters, 37, L20 502, https://doi.org/10.1029/2010GL044819, 2010.

Joughin, I., Smith, B. E., and Schoof, C. G.: Regularized Coulomb Friction Laws for Ice Sheet Sliding: Application to Pine Island Glacier, Antarctica, Geophysical Research Letters, 46, 4764–4771, https://doi.org/10.1029/2019GL082526, 2019.

https://doi.org/10.5194/egusphere-2026-343
Preprint. Discussion started: 3 March 2026

Jourdain, N. C., Asay-Davis, X., Hattermann, T., Straneo, F., Seroussi, H., Little, C. M., and Nowicki, S.: A protocol for calculating basal melt rates in the ISMIP6 Antarctic ice sheet projections, The Cryosphere, 14, 3111–3134, https://doi.org/10.5194/tc-14-3111-2020, 2020.

Kamb, B.: Glacier surge mechanism based on linked cavity configuration of the basal water conduit system, Journal of Geophysical Research: Solid Earth, 92, 9083–9100, https://doi.org/10.1029/JB092iB09p09083, 1987.

Kamb, B. and Echelmeyer, K. A.: Stress-Gradient Coupling in Glacier Flow: I. Longitudinal Averaging of the Influence of Ice Thickness and Surface Slope, Journal of Glaciology, 32, 267–284, https://doi.org/10.3189/S0022143000015604, 1986.

Kazmierczak, E., Gregov, T., Coulon, V., and Pattyn, F.: A fast and simplified subglacial hydrological model for the Antarctic Ice Sheet and outlet glaciers, The Cryosphere, 18, 5887–5911, https://doi.org/10.5194/tc-18-5887-2024, 2024.

Larour, E., Seroussi, H., Morlighem, M., and Rignot, E.: Continental scale, high order, high spatial resolution, ice sheet modeling using the Ice Sheet System Model (ISSM), Journal of Geophysical Research: Earth Surface, 117, F01 022, https://doi.org/10.1029/2011JF002140, 2012.

Livingstone, S. J., Li, Y., Rutishauser, A., Sanderson, R. J., Winter, K., Mikucki, J. A., Björnsson, H., Bowling, J. S., Chu, W., Dow, C. F., et al.: Subglacial lakes and their changing role in a warming climate, Nature Reviews Earth & Environment, 3, 106–124, 2022.

Lu, G. and Kingslake, J.: Two-way coupling between ice flow and channelized subglacial drainage enhances modeled marine-ice-sheet retreat, The Cryosphere, 18, 5301–5321, https://doi.org/10.5194/tc-18-5301-2024, 2024.

Lundberg, S. M. and Lee, S.-I.: A unified approach to interpreting model predictions, Advances in neural information processing systems, 30, 4765–4774, 2017.

Ma, Y., Zhao, L., Gladstone, R., Zwinger, T., Wolovick, M., Wang, J., and Moore, J. C.: Sensitivity of Totten Glacier dynamics to sliding parameterizations and ice shelf basal melt rates, The Cryosphere, 19, 6187–6205, https://doi.org/10.5194/tc-19-6187-2025, 2025.

MacAyeal, D. R.: Large-scale ice flow over a viscous basal sediment: Theory and application to ice stream B, Antarctica, Journal of Geophysical Research: Solid Earth, 94, 4071–4087, 1989.

Martos, Y. M., Catalán, M., Jordan, T. A., Golynsky, A., Golynsky, D., Eagles, G., and Vaughan, D. G.: Heat Flux Distribution of Antarctica Unveiled, Geophysical Research Letters, 44, 11 417–11 426, https://doi.org/10.1002/2017GL075609, 2017.

McArthur, K., McCormack, F. S., and Dow, C. F.: Basal conditions of Denman Glacier from glacier hydrology and ice dynamics modeling, The Cryosphere, 17, 4705–4727, https://doi.org/10.5194/tc-17-4705-2023, 2023.

Millstein, J. D., Minchew, B. M., and Pegler, S. S.: Ice viscosity is more sensitive to stress than commonly assumed, Communications Earth & Environment, 3, 57, https://doi.org/10.1038/s43247-022-00385-x, 2022.

Morlighem, M.: MEaSUREs BedMachine Antarctica, Version 3 [Dataset], https://doi.org/10.5067/FPSU0V1MWUB6, Date Accessed 2025-06-02, 2022.

Morlighem, M., Rignot, E., Seroussi, H., Larour, E., Ben Dhia, H., and Aubry, D.: Spatial patterns of basal drag inferred using control methods from a full-Stokes and simpler models for Pine Island Glacier, West Antarctica, Geophysical Research Letters, 37, L14 502, https://doi.org/10.1029/2010GL043853, 2010.

Morlighem, M., Rignot, E., Binder, T., Blankenship, D., Drews, R., Eagles, G., Eisen, O., Ferraccioli, F., Forsberg, R., Fretwell, P., et al.: Deep glacial troughs and stabilizing ridges unveiled beneath the margins of the Antarctic ice sheet, Nature geoscience, 13, 132–137, https://doi.org/10.1038/s41561-019-0510-8, 2020.

Murray, T. and Clarke, G. K. C.: Black-box modeling of the subglacial water system, Journal of Geophysical Research: Solid Earth, 100, 10 231–10 245, https://doi.org/10.1029/95JB00671, 1995.

https://doi.org/10.5194/egusphere-2026-343
Preprint. Discussion started: 3 March 2026

Muto, A., Alley, R. B., Parizek, B. R., and Anandakrishnan, S.: Bed-type variability and till (dis)continuity beneath Thwaites Glacier, West Antarctica, Annals of Glaciology, 60, 82–90, https://doi.org/10.1017/aog.2019.32, 2019.

Pedregosa, F., Varoquaux, G., Gramfort, A., Michel, V., Thirion, B., Grisel, O., Blondel, M., Prettenhofer, P., Weiss, R., Dubourg, V., Vanderplas, J., Passos, A., Cournapeau, D., Brucher, M., Perrot, M., and Duchesnay, E.: Scikit-learn: Machine Learning in Python, Journal of Machine Learning Research, 12, 2825–2830, 2011.

Pelle, T., Greenbaum, J. S., Dow, C. F., Jenkins, A., and Morlighem, M.: Subglacial discharge accelerates future retreat of Denman and Scott Glaciers, East Antarctica, Science Advances, 9, eadi9014, https://doi.org/10.1126/sciadv.adi9014, 2023.

Pelle, T., Greenbaum, J. S., Ehrenfeucht, S., Dow, C. F., and McCormack, F. S.: Subglacial Discharge Accelerates Dynamic Retreat of Aurora Subglacial Basin Outlet Glaciers, East Antarctica, Over the 21st Century, Journal of Geophysical Research: Earth Surface, 129, e2023JF007 513, https://doi.org/10.1029/2023JF007513, 2024.

Åkesson, H., Morlighem, M., O'Regan, M., and Jakobsson, M.: Future Projections of Petermann Glacier Under Ocean Warming Depend Strongly on Friction Law, Journal of Geophysical Research: Earth Surface, 126, e2020JF005 921, https://doi.org/10.1029/2020JF005921, 2021.

Raspoet, O. and Pattyn, F.: Estimates of basal and englacial thermal conditions of the Antarctic ice sheet, Journal of Glaciology, 71, e104, https://doi.org/10.1017/jog.2025.10087, 2025.

Rignot, E., Mouginot, J., and Scheuchl, B.: Antarctic grounding line mapping from differential satellite radar interferometry, Geophysical Research Letters, 38, L10 504, https://doi.org/10.1029/2011GL047109, 2011a.

Rignot, E., Mouginot, J., and Scheuchl, B.: Ice Flow of the Antarctic Ice Sheet, Science, 333, 1427–1430, https://doi.org/10.1126/science.1208336, 2011b.

Rignot, E., Mouginot, J., and Scheuchl, B.: MEaSUREs InSAR-Based Antarctica Ice Velocity Map. (NSIDC-0484, Version 2) [Dataset], https://doi.org/10.5067/D7GK8F5J8M8R, Date Accessed 2025-06-02, 2017.

Röthlisberger, H.: Water pressure in intra- and subglacial channels, Journal of Glaciology, 11, 177–203, https://doi.org/10.3189/S0022143000022188, 1972.

Schohn, C. M., Iverson, N. R., Zoet, L. K., Fowler, J. R., and Morgan-Witts, N.: Linear-viscous flow of temperate ice, Science, 387, 182–185, https://doi.org/10.1126/science.adp7708, 2025.

Schoof, C.: The effect of cavitation on glacier sliding, Proceedings of the Royal Society A: Mathematical, Physical and Engineering Sciences, 461, 609–627, https://doi.org/10.1098/rspa.2004.1350, 2005.

Schoof, C., Hewitt, I. J., and Werder, M. A.: Flotation and free surface flow in a model for subglacial drainage. Part 1. Distributed drainage, Journal of Fluid Mechanics, 702, 126–156, https://doi.org/10.1017/jfm.2012.165, 2012.

Seiner, O., Hugney, A., Seroussi, H., and MacGregor, J. A.: A synthesis of the basal thermal state of the Antarctic ice sheet, Journal of Glaciology, 127, e127, https://doi.org/10.1017/jog.2025.10102, 2025.

Seroussi, H., Pelle, T., Lipscomb, W. H., Abe-Ouchi, A., Albrecht, T., Alvarez-Solas, J., Asay-Davis, X., Barre, J.-B., Berends, C. J., Bernales, J., et al.: Evolution of the Antarctic Ice Sheet over the next three centuries from an ISMIP6 model ensemble, Earth's Future, 12, e2024EF004 561, https://doi.org/10.1029/2024EF004561, 2024.

Shreve, R. L.: Movement of Water in Glaciers, Journal of Glaciology, 11, 205–214, https://doi.org/10.3189/S002214300002219X, 1972.

Sommers, A., Rajaram, H., and Morlighem, M.: SHAKTI: subglacial hydrology and kinetic, transient interactions v1.0, Geoscientific Model Development, 11, 2955–2974, https://doi.org/10.5194/gmd-11-2955-2018, 2018.

https://doi.org/10.5194/egusphere-2026-343
Preprint. Discussion started: 3 March 2026

Vaňková, I., Asay-Davis, X. S., Begeman, C. B., Comeau, D., Hager, A. O., Hoffman, M. J., Price, S., and Wolfe, J. D.: Subglacial discharge effects on Antarctic ice-shelf basal melt and the Southern Ocean in a global, coupled ocean–sea-ice model, Journal of Geophysical Research: Oceans, 130, e2025JC022 999, https://doi.org/10.1029/2025JC022999, 2025.

Verjans, V. and Robel, A.: Accelerating Subglacial Hydrology for Ice Sheet Models With Deep Learning Methods, Geophysical Research Letters, 51, e2023GL105 281, https://doi.org/10.1029/2023GL105281, 2024.

Werder, M. A., Hewitt, I. J., Schoof, C. G., and Flowers, G. E.: Modeling channelized and distributed subglacial drainage in two dimensions, Journal of Geophysical Research: Earth Surface, 118, 2140–2158, https://doi.org/10.1002/jgrf.20146, 2013.

Wolovick, M., Humbert, A., Kleiner, T., and Rückamp, M.: Regularization and L-curves in ice sheet inverse models: a case study in the Filchner–Ronne catchment, The Cryosphere, 17, 5027–5060, https://doi.org/10.5194/tc-17-5027-2023, 2023.

Zhao, C., Gladstone, R., Zwinger, T., Gillet-Chaulet, F., Wang, Y., Caillet, J., Mathiot, P., Saraste, L., Jager, E., Galton-Fenzi, B. K., et al.: Subglacial water amplifies Antarctic contributions to sea-level rise, Nature Communications, 16, 3187, 2025.

Zoet, L. K. and Iverson, N. R.: A slip law for glaciers on deformable beds, Science, 368, 76–78, 2020.